Experimental and Numerical Investigation of a Parallel Jet MILD Combustion Burner System in a Laboratory-scale Furnace

by

George Gabriel Szegö

A thesis submitted in fulfilment of
the requirements for the degree of
Doctor of Philosophy

School of Mechanical Engineering
Faculty of Engineering, Mathematical and Computer Science

March 2010 (Approved in July 2010)

Bibliography

[1] ABB Instrumentation, Variable Area Flowmeter, Glass Tube Models A3500 and A3600, ABB (2000).

[2] J. B. Adolfi, C. Ellul, S. Santos, F. Frinking, P. Hoppesteyn, Experimental results from the HEC-EEC furnace and burners firing natural gas, Tech. Rep. IFRF Doc. No. F108/y/2, International Flame Research Foundation (September 2004).

[3] S. Afsharvahid, P. J. Ashman, B. B. Dally, Investigation of NO_x conversion characteristics in a porous medium, Combustion and Flame 152 (4) (2008) 604–615.

[4] C. Ahn, F. Akamatsu, M. Katsuki, A. Kitajima, The influences of mixture composition and preheat temperature on combustion regime and flame structure of premixed turbulent flames, in: The Fourth Asia-Pacific Conference on Combustion, The Combustion Institute, China, 2003, pp. 40–43.

[5] Y. M. Al-Abdeli, A. R. Masri, G. R. Marquez, S. H. Starner, Time-varying behaviour of turbulent swirling nonpremixed flames, Combustion and Flame 146 (1-2) (2006) 200–214.

[6] A. D. Al-Fawaz, L. M. Dearden, J. T. Hedley, M. Missaghi, M. Pourkashanian, A. Williams, L. T. Yap, NO_x formation in geometrically scaled gas-fired industrial burners, Proceedings of the Combustion Institute 25 (1994) 1027–1034.

[7] H.-E. Albrecht, N. Damaschke, M. Borys, C. Tropea, Laser Doppler and

Phase Doppler Measurement Techniques, Experimental fluid mechanics, 1st ed., Springer, New York, 2003.

[8] R. Ancimer, R. Fraser, Flame-induced laser Doppler velocimetry velocity bias, Measurement Science and Technology (5) (1994) 83–92.

[9] I. O. Awosope, N. H. Kandamby, F. C. Lockwood, Flameless oxidation modelling: On application to gas turbine combustors, Journal of the Energy Institute 79 (2) (2006) 75–83.

[10] I. O. Awosope, F. C. Lockwood, Prediction of combustion and NO_x emission characteristics of flameless oxidation combustion, IFRF Combustion Journal Article Number 200501.

[11] J. Baltasar, M. G. Carvalho, P. Coelho, M. Costa, Flue gas recirculation in a gas-fired laboratory furnace: Measurements and modelling, Fuel 76 (10) (1997) 919–929.

[12] C. Baukal, Oxygen-Enhanced Combustion, 1st ed., CRC Press LLC, New York, NY, 1998.

[13] J. M. Beer, Combustion technology developments in power generation in response to environmental challenges, Progress in Energy and Combustion Science 26 (4-6) (2000) 301–327.

[14] J. M. Beer, High efficiency electric power generation: The environmental role, Progress in Energy and Combustion Science 33 (2) (2007) 107–134.

[15] F. K. Besik, S. Rahbar, H. A. Becker, A. Sobiesiak, Low NO_x burner (June 30 1998).

[16] R. Bilger, S. Stårner, R. Kee, On reduced mechanisms for methane-air combustion in nonpremixed flames, Combustion and Flame 80 (2) (1990) 135–149.

[17] J. Bluestein, NO_x controls for gas-fired industrial boilers and combustion equipment: A survey of current practices, Tech. Rep. GRI-92/0374, Gas Research Institute, Chicago, IL (1992).

[18] R. Borghi, Turbulent combustion modelling, Progress in Energy and Combustion Science 14 (4) (1988) 245–292.

[19] G. L. Borman, K. W. Ragland, Combustion engineering, McGraw-Hill, Boston, 1998.

[20] C. T. Bowman, Control of combustion-generated nitrogen oxide emissions: Technology driven by regulation, Proceedings of the Combustion Institute 24 (1) (1992) 859–878.

[21] R. Cabra, T. Myhrvold, J. Y. Chen, R. W. Dibble, A. N. Karpetis, R. S. Barlow, Simultaneous laser Raman-Rayleigh-LIF measurements and numerical modeling results of a lifted turbulent H_2/N_2 jet flame in a vitiated coflow, Proceedings of the Combustion Institute 29 (2) (2002) 1881–1888.

[22] B. E. Cain, T. F. Robertson, J. N. Newby, Low NO_x combustion method and apparatus (October 28 2003).

[23] A. Cavaliere, M. De Joannon, MILD combustion, Progress in Energy and Combustion Science 30 (4) (2004) 329–366.

[24] A. Cavaliere, M. De Joannon, R. Ragucci, Lean Combustion: Technology and Control, chap. 3: Highly Preheated Lean Combustion, 1st ed., Academic Press, 2007.

[25] A. Cavigiolo, M. A. Galbiati, A. Effuggi, D. Gelosa, R. Rota, Mild combustion in a laboratory-scale apparatus, Combustion Science and Technology 175 (8) (2003) 1347–1367.

[26] G.-M. Choi, M. Katsuki, Advanced low NO_x combustion using highly preheated air, Energy Conversion and Management 42 (5) (2001) 639–652.

[27] G.-M. Choi, M. Katsuki, Chemical kinetic study on the reduction of nitric oxide in highly preheated air combustion, Proceedings of the Combustion Institute 29 (2002) 1165–1171.

[28] F. Christo, B. Dally, Modeling turbulent reacting jets issuing into a hot and diluted coflow, Combustion and Flame 142 (1-2) (2005) 117–129.

[29] F. Christo, G. Szegö, B. Dally, Modeling turbulent reacting jets under MILD combustion conditions, in: The Fifth Asia-Pacific Conference on Combustion, The Combustion Institute, Adelaide, Australia, 2005, pp. 329–332.

[30] F. Christo, G. Szegö, B. Dally, Molecular fluxes effect on predictions of JHC flames, in: The Sixth Asia-Pacific Conference on Combustion, The Combustion Institute, Nagoya, Japan, 2007, pp. 448–451.

[31] F. C. Christo, B. B. Dally, Application of transport PDF approach for modelling MILD combustion, in: 15th Australasian Fluid Mechanics Conference, The University of Sydney, Sydney, Australia, 2004.

[32] P. Coelho, N. Peters, Numerical simulation of a mild combustion burner, Combustion and Flame 124 (2001) 503–518.

[33] S. M. Correa, A review of NO_x formation under gas-turbine combustion conditions, Combustion Science and Technology 87 (1) (1993) 329–362.

[34] M. Costa, C. Parente, A. Santos, Nitrogen oxides emissions from buoyancy and momentum controlled turbulent methane jet diffusion flames, Experimental Thermal and Fluid Science 28 (7) (2004) 729–734.

[35] P. Dagaut, A. Nicolle, Experimental study and detailed kinetic modeling of the effect of exhaust gas on fuel combustion: mutual sensitization of the oxidation of nitric oxide and methane over extended temperature and pressure ranges, Combustion and Flame 140 (3) (2005) 161–171.

[36] B. Dally, N. Peters, Heat loss-induced oscillation of methane and ethylene in a perfectly stirred reactor, in: The Sixth Asia-Pacific Conference on Combustion, The Combustion Institute, Nagoya, Japan, 2007, pp. 227–230.

[37] B. Dally, E. Riesmeier, N. Peters, Effect of fuel mixture on moderate and intense low oxygen dilution combustion, Combustion and Flame 137 (4) (2004) 418–431.

[38] B. B. Dally, A. Karpetis, R. Barlow, Structure of jet laminar nonpremixed flames under diluted hot coflow conditions, in: Australian Symposium on Combustion and The Seventh Australian Flame Days, Adelaide, Australia, 2002.

[39] B. B. Dally, A. N. Karpetis, R. S. Barlow, Structure of turbulent nonpremixed jet flames in a diluted hot coflow, Proceedings of the Combustion Institute 29 (1) (2002) 1147–1154.

[40] Dantec Dynamics, BSA Flow Software v2: Installation and User's guide, Tonsbakken 18, DK-2740 Skovlunde, Denmark, 2002.

[41] J. Davis, Statistics and Data Analysis in Geology, John Wiley, New York, 1986.

[42] M. De Joannon, A. Cavaliere, T. Faravelli, E. Ranzi, P. Sabia, A. Tregrossi, Analysis of process parameters for steady operations in methane mild combustion technology, Proceedings of the Combustion Institute 30 (2) (2005) 2605–2612.

[43] M. De Joannon, G. Langella, F. Beretta, A. Cavaliere, C. Noviello, Mild combustion: Process features and technological constrains, Combustion Science and Technology 153 (1) (2000) 33–50.

[44] M. De Joannon, P. Sabia, A. Tregrossi, A. Cavaliere, Dynamic behavior of methane oxidation in premixed flow reactor, Combustion Science and Technology 176 (5-6) (2004) 769–783.

[45] M. De Joannon, A. Saponaro, A. Cavaliere, Zero-dimensional analysis of diluted oxidation of methane in rich conditions, Proceedings of the Combustion Institute 28 (2000) 1639–1645.

[46] G. G. De Soete, Overall reaction rates of NO and N_2 formation from fuel nitrogen, Proceedings of the Combustion Institute 15 (1975) 1093–1102.

[47] A. M. Dean, J. W. Bozzelli, Gas-phase combustion chemistry - Combustion Chemistry of Nitrogen, chap. 2, Springer, 2000, p. 543.

[48] L. I. Díez, C. Cortés, J. Pallarés, Numerical investigation of NO_x emissions from a tangentially-fired utility boiler under conventional and overfire air operation, Fuel 87 (7) (2008) 1259–1269.

[49] P. Domingo, L. Vervisch, D. Veynante, Large-eddy simulation of a lifted methane jet flame in a vitiated coflow, Combustion and Flame 152 (3) (2008) 415–432.

[50] J. M. Donelan, Q. Li, V. Naing, J. A. Hoffer, D. J. Weber, A. D. Kuo, Biomechanical energy harvesting: Generating electricity during walking with minimal user effort, Science 319 (5864) (2008) 807–810.

[51] J. F. Driscoll, R.-H. Chen, Y. Yoon, Nitric oxide levels of turbulent jet diffusion flames: Effects of residence time and damkohler number, Combustion and Flame 88 (1) (1992) 37–49.

[52] M. J. Dunn, A. R. Masri, R. W. Bilger, A new piloted premixed jet burner to study strong finite-rate chemistry effects, Combustion and Flame 151 (1-2) (2007) 46–60.

[53] F. Durst, A. Melling, J. H. Whitelaw, Principles and practice of laser-Doppler anemometry, 2nd ed., Academic Press, London ; New York, 1981.

[54] C. Duwig, D. Stankovic, L. Fuchs, G. Li, E. Gutmark, Experimental and numerical study of flameless combustion in a model gas turbine combustor, Combustion Science and Technology 180 (2) (2008) 279–295.

[55] A. Effuggi, D. Gelosa, M. Derudi, R. Rota, Mild combustion of methane-derived fuel mixtures: Natural gas and biogas, Combustion Science and Technology 180 (3) (2008) 481–493.

[56] Energy Information Administration, International energy outlook 2007, Tech. Rep. DOE/EIA-0484(2007), U.S. Department of Energy (May 2007).

[57] P. Evrard, B. Pesenti, P. Lybaert, NO_x production and radiative heat transfer from an autoregenerative flameless oxidation burner, in: 6th European Conference on Industrial Furnaces and Boilers, Portugal, 2002.

[58] C. P. Fenimore, Formation of nitric oxide in premixed hydrocarbon flames, Proceedings of the Combustion Institute 13 (1) (1971) 373–380.

[59] M. Flamme, Low NO_x combustion technologies for high temperature applications, Energy Conversion and Management 42 (15-17 Oct 1) (2001) 1919–1935.

[60] M. Flamme, New combustion systems for gas turbines (ngt), Applied Thermal Engineering 24 (11-12) (2004) 1551–1559.

[61] B. Fleck, A. Sobiesiak, H. Becker, Experimental and numerical investigation of the novel low NO_x CGRI burner, Combustion Science and Technology 161 (1-6) (2000) 89–112.

[62] FLUENT INC., FLUENT 6.3 User's Guide, Lebanon NH 03766, USA, 2006.

[63] FLUENT INC., GAMBIT 2.3 User's Guide, Lebanon NH 03766, USA, 2006.

[64] F. Frinking, Laser based measurements of HEC-EEC burners and furnace, Tech. Rep. IFRF Doc. no F108/y/1, International Flame Research Foundation (2004).

[65] T. Fujimori, Y. Hamano, J. Sato, Radiative heat loss and NO_x emission of turbulent jet flames in preheated air up to 1230 k, Proceedings of the Combustion Institute 28 (1) (2000) 455–461.

[66] J. Furukawa, H. Hashimoto, S. Mochida, T. Hasegawa, Local reaction zone structure of non-premixed flames of propane with highly preheated low-oxygen air, Combustion Science and Technology 179 (4) (2007) 723–745.

[67] C. Galletti, A. Parente, L. Tognotti, Numerical and experimental investigation of a mild combustion burner, Combustion and Flame 151 (4) (2007) 649–664.

[68] K. Gkagkas, K. Goh, R. P. Lindstedt, Chemical kinetics for flameless combustion, in: Flameless Combustion Workshop, Lund University, Lund, Sweden, 2005.

[69] K. Gkagkas, R. P. Lindstedt, Transported pdf modelling with detailed chemistry of pre- and auto-ignition in ch4/air mixtures, Proceedings of the Combustion Institute 31 (1) (2007) 1559–1566.

[70] P. Glarborg, M. U. Alzueta, K. Dam-Johansen, J. A. Miller, Kinetic modeling of hydrocarbon/nitric oxide interactions in a flow reactor, Combustion and Flame 115 (1-2) (1998) 1–27.

[71] M. Glass, I. M. Kennedy, An improved seeding method for high temperature laser doppler velocimetry, Combustion and Flame 29 (1977) 333–335.

[72] I. Glassman, Combustion, 3rd ed., Academic Press, 1996.

[73] R. L. Gordon, A numerical and experimental investigation of autoignition, Ph.D. thesis, University of Sydney, School of Aerospace, Mechanical and Mechatronic Engineering (April 2008).

[74] R. L. Gordon, A. R. Masri, E. Mastorakos, Simultaneous rayleigh temperature, oh- and ch2o-lif imaging of methane jets in a vitiated coflow, Combustion and Flame 155 (1-2) (2008) 181–195.

[75] R. L. Gordon, A. R. Masri, S. B. Pope, G. M. Goldin, A numerical study of auto-ignition in turbulent lifted flames issuing into a vitiated co-flow, Combustion Theory and Modelling 11 (3) (2007) 351–376.

[76] R. L. Gordon, A. R. Masri, S. B. Pope, G. M. Goldin, Transport budgets in turbulent lifted flames of methane autoigniting in a vitiated co-flow, Combustion and Flame 151 (3) (2007) 495–511.

[77] S. Gordon, B. J. McBride, Computer program for calculation of complex chemical equilibrium compositions and applications, Tech. Rep. NASA RP-1311, NASA Lewis Research Center, Cleveland, Ohio 44135-3191 (October 1994).

[78] N. Goren-Inbar, N. Alperson, M. E. Kislev, O. Simchoni, Y. Melamed, A. Ben-Nun, E. Werker, Evidence of hominin control of fire at gesher benot ya'aqov, israel, Science 304 (5671) (2004) 725–727.

[79] E. W. Grandmaison, I. Yimer, H. A. Becker, A. Sobiesiak, Strong-jet/weak-jet problem and aerodynamic modeling of the CGRI burner, Combustion and Flame 114 (3-4) (1998) 381–396.

[80] J. F. Griffiths, J. A. Barnard, Flame and combustion, 3rd ed., Chapman and Hall (Blackie Academic and Professional), Glasgow, 1995.

[81] A. K. Gupta, Flame characteristics and challenges with high temperature air combustion, in: Proceedings of ASME International Joint Power Generation Conference and Exposition, Florida, USA, 2000.

[82] A. Gurney, M. Ford, K. Low, C. Tulloh, G. Jakeman, D. Gunasekera, Technology: Toward a low emissions future, Tech. Rep. Research Report 07.16, ABARE, Canberra, Australia (September 2007).

[83] E. Hampartsoumian, D. Hainsworth, J. Taylor, A. Williams, The radiant emissivity of some materials at high temperatures, Journal of the Institute of Energy 74 (2001) 91.

[84] D. R. Hardesty, F. J. Weinberg, Burners producing large excess enthalpies, Combustion Science and Technology 8 (5-6) (1974) 201–214.

[85] T. T. Hasegawa, T. R. Niioka, Combustion with high temperature low oxygen air in regenerative burners, in: The First Asia-Pacific Conference on Combustion, Osaka, Japan, 1997, pp. 290–293.

[86] R. H. Hekkens, Isothermal CFD model of HEC burner and furnace, Tech. Rep. IFRF Doc. no G108/y/1, International Flame Research Foundation (July 2004).

[87] R. H. Hekkens, Non-isothermal CFD model of the HEC burner and furnace (Additional Calculation), Tech. Rep. IFRF Doc. no G108/y/3, International Flame Research Foundation (November 2004).

[88] R. H. Hekkens, M. Mancini, Non-isothermal CFD model of the HEC burner and furnace, Tech. Rep. IFRF Doc. no G108/y/2, International Flame Research Foundation (September 2004).

[89] J. B. Heywood, Internal Combustion Engine Fundamentals, McGraw-Hill series in mechanical engineering, 1st ed., McGraw-Hill, New York, 1988.

[90] T. C. A. Hsieh, W. J. A. Dahm, J. F. Driscoll, Scaling laws for NO_x emission performance of burners and furnaces from 30 kW to 12 MW, Combustion and Flame 114 (1-2) (1998) 54–80.

[91] F. P. Incropera, D. P. DeWitt, Fundamentals of heat and mass transfer, 4th ed., Wiley, New York, 1996.

[92] IPCC, Climate Change 2007: Mitigation. Contribution of Working Group III to the Fourth Assessment Report of the Intergovernmental Panel on Climate Change, vol. 3, Cambridge University Press, Cambridge, United Kingdom and New York, NY, USA, Geneva, Switzerland, 2007.

[93] IPCC, Climate Change 2007: The Physical Science Basis. Contribution of Working Group I to the Fourth Assessment Report of the Intergovernmental Panel on Climate Change, vol. 1, Cambridge University Press, Cambridge, United Kingdom and New York, NY, USA, Geneva, Switzerland, 2007.

[94] T. Ishiguro, S. Tsuge, T. Furuhata, K. Kitagawa, N. Arai, T. Hasegawa, R. Tanaka, A. K. Gupta, Homogenization and stabilization during combustion of hydrocarbons with preheated air, Proceedings of the Combustion Institute 27 (2) (1998) 3205–3213.

[95] T. Ishii, C. Zhang, S. Sugiyama, Effects of NO models on the prediction of NO formation in a regenerative furnace, Journal of Energy Resources Technology 122 (4) (2000) 224–228.

[96] ISO 6976:1995, Natural gas – Calculation of calorific values, density, relative density and Wobbe index from composition (1995).

[97] W. P. Jones, R. P. Lindstedt, Global reaction schemes for hydrocarbon combustion, Combustion and Flame 73 (3) (1988) 233–249.

[98] M. Katsuki, T. Hasegawa, The science and technology of combustion in highly preheated air, Proceedings of the Combustion Institute 27 (1998) 3135–3146.

[99] J. P. Kim, U. Schnell, G. Scheffknecht, Comparison of different global reaction mechanisms for mild combustion of natural gas, Combustion Science and Technology 180 (4) (2008) 565–592.

[100] S. H. Kim, K. Y. Huh, B. Dally, Conditional moment closure modeling of turbulent nonpremixed combustion in diluted hot coflow, Proceedings of the Combustion Institute 30 (1) (2005) 751–757.

[101] A. Kitajima, T. Hatanaka, M. Takeuchi, H. Torikai, T. Miyadera, Experimental study of PAH formation in laminar counterflow CH_4-N_2/O_2-N_2 and C_3H_8-N_2/O_2-N_2 nonpremixed flames, Combustion and Flame 142 (1-2) (2005) 72–88.

[102] J. Kitto, S. Stultz, Steam: Its generation and use, The Babcock & Wilcox Company, 2005.

[103] H. Kobayashi, K. Yoshikawa, Thermal performance and numerical simulation of high temperature air combustion boiler, in: Proceedings of 2000 International Joint Power Generation Conference, Miami Beach, Florida, 2000.

[104] N. Krishnamurthy, W. Blasiak, A. Lugnet, Development of high temperature air and oxy-fuel combustion technologies for minimized CO_2 and NO_x emissions in industrial heating, in: The Joint International Conference on Sustainable Energy and Environment, Hua Hin, Thailand, 2004.

[105] S. Kumar, P. Paul, H. Mukunda, Studies on a new high-intensity low-emission burner, Proceedings of the Combustion Institute 29 (2002) 1131–1137.

[106] S. Kumar, P. J. Paul, H. S. Mukunda, Investigations of the scaling criteria for a mild combustion burner, Proceedings of the Combustion Institute 30 (2) (2005) 2613–2621.

[107] S. Kumar, P. J. Paul, H. S. Mukunda, Prediction of flame liftoff height of diffusion/partially premixed jet flames and modeling of mild combustion burners, Combustion Science and Technology 179 (10) (2007) 2219–2253.

[108] F. Lainault, T. Ferlin, Applied research, development and services for the optimization of natural gas utilization in the field of glass melting furnaces, International Glass Journal 2004 (133) (2004) 32–37.

[109] D. Lentini, I. K. Puri, Stretched laminar flamelet modeling of turbulent chloromethane-air nonpremixed jet flames, Combustion and Flame 103 (4) (1995) 328–338.

[110] Y. Levy, V. Sherbaum, P. Arfi, Basic thermodynamics of FLOXCOM, the low-NO_x gas turbines adiabatic combustor, Applied Thermal Engineering 24 (11-12) (2004) 1593–1605.

[111] Y. N. V. Levy, A. Nekrusov, Experimental unit for investigation flameless oxidation NO_x reduction in gas turbines, Tech. Rep. JTL001-02-2003, Technion Israel Institute of Technology (2003).

[112] J. Li, Z. Zhao, A. Kazakov, F. L. Dryer, An updated comprehensive kinetic model of hydrogen combustion, International Journal of Chemical Kinetics 36 (10) (2004) 566–575.

[113] S. Lille, W. Blasiak, M. Jewartowski, Experimental study of the fuel jet combustion in high temperature and low oxygen content exhaust gases, Energy 30 (2-4) (2005) 373–384.

[114] R. P. Lindstedt, S. A. Louloudi, E. M. Váos, Joint scalar probability density function modeling of pollutant formation in piloted turbulent jet diffusion flames with comprehensive chemistry, Proceedings of the Combustion Institute 28 (1) (2000) 149–156.

[115] R. P. Lindstedt, V. Sakthitharan, Time resolved velocity and turbulence measurements in turbulent gaseous explosions, Combustion and Flame 114 (3-4) (1998) 469–483.

[116] G. Löffler, V. J. Wargadalam, F. Winter, H. Hofbauer, Decomposition of nitrous oxide at medium temperatures, Combustion and Flame 120 (4) (2000) 427–438.

[117] D. Lupant, B. Pesenti, P. Evrard, P. Lybaert, Numerical and experimental characterization of a self-regenerative flameless oxidation burner operation in a pilot-scale furnace, Combustion Science and Technology 179 (1) (2007) 437–453.

[118] D. Lupant, B. Pesenti, P. Lybaert, Assessment of combustion models of a self-regenerative flameless oxidation burner, in: Proceedings of the 7th European Conference on Industrial Furnaces and Boilers, CENERTEC - Centro de Energia e Tecnologia, Ltda., Porto, Portugal, 2006.

[119] B. F. Magnussen, On the structure of turbulence and a generalized eddy dissipation concept for chemical reaction in turbulent flow, in: AIAA 19th Aerospace Science Meeting, St.Louis, Missouri., 1981.

[120] B. F. Magnussen, B. H. Hjertager, On mathematical modeling of turbulent combustion with special emphasis on soot formation and combustion, Proceedings of the Combustion Institute 16 (1) (1977) 719–729.

[121] P. C. Malte, D. T. Pratt, Measurement of atomic oxygen and nitrogen oxides in jet-stirred combustion, Proceedings of the Combustion Institute 15 (1) (1974) 1061–1070.

[122] M. Mancini, P. Schwoppe, R. Weber, S. Orsino, On mathematical modelling of flameless combustion, Combustion and Flame 150 (1-2) (2007) 54–59.

[123] M. Mancini, R. Weber, U. Bollettini, Predicting NO_x emissions of a burner operated in flameless oxidation mode, Proceedings of the Combustion Institute 29 (2002) 1155–1162.

[124] N. M. Marinov, W. J. Pitz, C. K. Westbrook, A. M. Vincitore, M. J. Castaldi, S. M. Senkan, C. F. Melius, Aromatic and polycyclic aromatic hydrocarbon formation in a laminar premixed n-butane flame, Combustion and Flame 114 (1-2) (1998) 192–213.

[125] P. B. Martin, G. J. Pugliese, J. G. Leishman, Laser doppler velocimetry uncertainty analysis for rotor blade tip vortex measurements, in: AIAA 38th Aerospace Science Meeting, No. 2000-0263, American Institute of Aeronautics and Astronautics, 2000.

[126] E. Mastorakos, A. Taylor, J. Whitelaw, Extinction of turbulent counterflow flames with reactants diluted by hot products, Combustion and Flame 102 (1-2) (1995) 101–114.

[127] M. Matsumoto, I. Nakamachi, S. Yasuoka, N. Saiki, T. Koizumi, Advanced fuel direct injection - FDI system, in: 11th IFRF Members Conference, 1995.

[128] A. Matysek, M. Ford, G. Jakeman, A. Gurney, B. Fisher, Technology: Its role in economic development and climate change, Tech. Rep. Research Report 06.6, ABARE, Canberra, Australia (July 2006).

[129] P. R. Medwell, Laser diagnostics in mild combustion, Ph.D. thesis, University of Adelaide, School of Mechanical Engineering (October 2007).

[130] P. R. Medwell, P. A. M. Kalt, B. B. Dally, Simultaneous imaging of OH, formaldehyde, and temperature of turbulent nonpremixed jet flames in a heated and diluted coflow, Combustion and Flame 148 (1-2) (2007) 48–61.

[131] P. R. Medwell, P. A. M. Kalt, B. B. Dally, Imaging of diluted turbulent ethylene flames stabilized on a jet in hot coflow (JHC) burner, Combustion and Flame 152 (1-2) (2008) 100–113.

[132] J. B. Mereb, J. O. L. Wendt, Air staging and reburning mechanisms for NO_x abatement in a laboratory coal combustor, Fuel 73 (7) (1994) 1020–1026.

[133] A. Milani, A. Saponaro, Diluted combustion technology, IFRF Combustion Journal Article Number 200101.

[134] A. Milani, J. Wünning, Radiant tube technology for strip line furnaces, IFRF Combustion Journal Article Number 200405.

[135] J. A. Miller, C. T. Bowman, Mechanism and modeling of nitrogen chemistry in combustion, Progress in Energy and Combustion Science 15 (4) (1989) 287–338.

[136] M. Mortberg, W. Blasiak, A. K. Gupta, Combustion of normal and low calorific fuels in high temperature and oxygen deficient environment, Combustion Science and Technology 178 (7) (2006) 1345–1372.

[137] I. Nakamachi, K. Yasuzawa, T. Miyahara, T. Nagata, Apparatus or method for carrying out combustion in a furnace (Aug. 7 1990).

[138] G. J. Nathan, R. E. Luxton, J. P. Smart, Reduced NO_x emissions and enhanced large scale turbulence from a precessing jet burner, Proceedings of the Combustion Institute 24 (1992) 1399–1405.

[139] G. J. R. Newbold, G. J. Nathan, D. S. Nobes, S. R. Turns, Measurement and prediction of NO_x emissions from unconfined propane flames from turbulent-jet, bluff-body, swirl, and precessing jet burners, Proceedings of the Combustion Institute 28 (1) (2000) 481–487.

[140] J. Newby, B. Cain, T. Robertson, The development and application of direct fuel injection techniques for emissions reduction in high temperature furnaces, in: Proceedings of the 2nd International Seminar on High Temperature Combustion In Industrial Furnaces, Stockholm, Sweden, 2000.

[141] A. Nicolle, P. Dagaut, Occurrence of NO-reburning in mild combustion evidenced via chemical kinetic modeling, Fuel 85 (17-18) (2006) 2469–2478.

[142] M. Nishimura, T. Suzuki, R. Nakanishi, R. Kitamura, Low-NO_x combustion under high preheated air temperature condition in an industrial furnace, Energy Conversion and Management 38 (10-13) (1997) 1353–1363.

[143] M. Oberlack, R. Arlitt, N. Peters, On stochastic Damköhler number variations in a homogeneous flow reactor, Combustion Theory and Modelling 4 (4) (2000) 495–509.

[144] OECD/IEA, CO_2 emissions from fuel combustion: 1971-2000, IEA statistics, Organisation for Economic Co-operation and Development and International Energy Agency, Paris, 2002.

[145] OECD/IEA, World energy outlook 2006, Organisation for Economic Co-operation and Development and International Energy Agency, Paris, France, 2006.

[146] S. Orsino, R. Weber, U. Bollettini, Numerical simulation of combustion of natural gas with high-temperature air, Combustion Science and Technology 170 (1) (2001) 1–34.

[147] I. Özdemir, N. Peters, Characteristics of the reaction zone in a combustor operating at mild combustion, Experiments in Fluids 30 (6) (2001) 683–695.

[148] G. P. Smith, D. M. Golden, M. Frenklach, N. W. Moriarty, B. Eiteneer, M. Goldenberg, C. T. Bowman, R. K. Hanson, S. Song, W. C. J. Gardiner, V. V. Lissianski, Z. Qin, GRI mechanism 3.0.

[149] S. Pacala, R. Socolow, Stabilization wedges: Solving the climate problem for the next 50 years with current technologies, Science 305 (5686) (2004) 968–972.

[150] J. Park, J.-W. Choi, S.-G. Kim, K.-T. Kim, S.-I. Keel, D.-S. Noh, Numerical study on steam-added mild combustion, International Journal of Energy Research 28 (13) (2004) 1197–1212.

[151] N. Peters, Laminar diffusion flamelet models in non-premixed turbulent combustion, Progress in Energy and Combustion Science 10 (3) (1984) 319–339.

[152] N. Peters, Turbulent combustion, Cambridge monographs on mechanics, Cambridge University Press, Cambridge, 2000.

[153] O. Piepers, P. Breithaupt, A. Van Beelen, Stability of flames close to auto-ignition temperatures generated by extreme separated gas-air inlets, Journal of Energy Resources Technology, Transactions of the ASME 123 (1) (2001) 50–58.

[154] T. Plessing, N. Peters, J. G. Wuenning, Laseroptical investigation of highly preheated combustion with strong exhaust gas recirculation, Proceedings of the Combustion Institute 27 (1998) 3197–3204.

[155] D. Poirier, E. Grandmaison, A. Lawrence, M. Matovic, E. Boyd, Oxygen-enriched combustion studies with the low NO_x CGRI burner, IFRF Combustion Journal Article Number 200404.

[156] S. B. Pope, Computationally efficient implementation of combustion chemistry using in situ adaptive tabulation, Combustion Theory and Modelling 1 (1997) 41–63.

[157] G. D. Raithby, E. H. Chui, A finite-volume method for predicting a radiant heat transfer in enclosures with participating media, Journal of Heat Transfer 112 (2) (1990) 415–423.

[158] J. Raub, Carbon monoxide, 2nd ed., International Programme on Chemical Safety (IPCS), Geneva, Switzerland, 1999.

[159] J. M. Rhine, R. J. Tucker, Modelling of gas-fired furnaces and boilers and other industrial heating processes, British Gas; McGraw-Hill, London, 1991.

[160] D. Riechelmann, T. Fujimori, J. Sato, Effect of dilution on extinction of methane diffusion flame in high temperature air up to 1500 K, Combustion Science and Technology 174 (2) (2002) 23–46.

[161] N. A. Røkke, J. E. Hustad, O. K. Sønju, F. A. Williams, Scaling of nitric oxide emissions from buoyancy-dominated hydrocarbon turbulent-jet diffusion flames, Proceedings of the Combustion Institute 24 (1992) 385–393.

[162] M. Rudd, New theoretical model for laser dopplermeter, Journal of Scientific Instruments Series 2 2 (1) (1969) 55 – 58.

[163] P. Sabia, M. de Joannon, S. Fierro, A. Tregrossi, A. Cavaliere, Hydrogen-enriched methane mild combustion in a well stirred reactor, Experimental Thermal and Fluid Science 31 (5) (2007) 469–475.

[164] T. Sano, NO_2 formation in the mixing region of hot burned gas with cool air, Combustion Science and Technology 38 (3) (1984) 129–144.

[165] A. Sayre, N. Lallemant, J. Dugue, R. Weber, Effect of radiation on nitrogen oxide emissions from nonsooty swirling flames of natural gas, Proceedings of the Combustion Institute 25 (1) (1994) 235–242.

[166] S. H. Shim, B. B. Dally, P. J. Ashman, G. G. Szegö, R. Craig, Sawdust application to mild combustion, in: Proceedings of the Australian Combustion Symposium, University of Sydney, 2007, pp. 94–97.

[167] N. Shimo, Y. Koyama, K. Yoshikawa, Low NO_x combustion of petroleum with highly preheated air - inluences of fuel properties, in: Proceedings of 2000 International Joint Power Generation Conference, Miami Beach, Florida, 2000.

[168] R. Siegel, J. R. Howell, Thermal radiation heat transfer, 4th ed., Taylor and Francis, New York, 2002.

[169] T. F. Smith, Z. F. Shen, J. N. Friedman, Evaluation of coefficients for the weighted sum of gray gases model, Journal of Heat Transfer 104 (4) (1982) 602–608.

[170] M. D. Smooke, I. K. Puri, K. Seshadri, A comparison between numerical calculations and experimental measurements of the structure of a counterflow diffusion flame burning diluted methane in diluted air, Proceedings of the Combustion Institute 21 (1) (1986) 1783–1792.

[171] A. Sobiesiak, S. Rahbar, H. A. Becker, Performance characteristics of the novel low-NO_x CGRI burner for use with high air preheat, Combustion and Flame 115 (1-2) (1998) 93–125.

[172] D. B. Spalding, Mixing and chemical reaction in steady confined turbulent flames, Proceedings of the Combustion Institute 13 (1) (1971) 649–657.

[173] R. C. Steele, P. C. Malte, D. G. Nicol, J. C. Kramlich, NO_x and N_2O in lean-premixed jet-stirred flames, Combustion and Flame 100 (3) (1995) 440–449.

[174] N. H. Stern, The economics of climate change : the Stern Review, Cambridge University Press, 2007.

[175] P. Struk, D. Dietrich, R. Valentine, I. Feier, Comparisons of gas-phase temperature measurements in a flame using thin-filament pyrometry and thermocouples, Tech. Rep. TM-2003-212096 / AIAA-2003-853, NASA (February 2003).

[176] C. J. Sung, J. S. Kistler, M. Nishioka, C. K. Law, Further studies on effects of thermophoresis on seeding particles in LDV measurements of strained flames, Combustion and Flame 105 (1-2) (1996) 189–201.

[177] C. J. Sung, C. K. Law, J. Y. Chen, Augmented reduced mechanisms for NO emission in methane oxidation, Combustion and Flame 125 (1-2) (2001) 906–919.

[178] T. Suzuki, K. Morimoto, K. Otani, T. Yamagata, R. Odawara, T. Fukuda, Development of high efficiency burners with low NO_x emission, Journal of the Institute of Energy 55 (425) (1982) 212–215.

[179] G. G. Szegö, B. B. Dally, G. J. Nathan, F. C. Christo, Design optimisation of a MILD combustion furnace based on CFD modelling, in: D. Honnery (ed.), Proceedings of the 2003 Australian Symposium on Combustion and the Eighth Australian Flame Days, No. P047, Monash University, Melbourne, 2003.

[180] D. Tabacco, C. Innarella, C. Bruno, Theoretical and numerical investigation on flameless combustion, Combustion Science and Technology 174 (7) (2002) 1–35.

[181] D. Teraji, Mercury 50 field evaluation and product introduction, in: Sixteenth Symposium on Industrial Application of Gas Turbines (IAGT), No. Paper No: 05-IAGT-1.1, Banff, Alberta, Canada, 2005.

[182] H. Tsuji, M. Morita, A. K. Gupta, M. Katsuki, K. Kishimoto, T. Hasegawa, High Temperature Air Combustion: From Energy Conservation to Pollution Reduction, Environmental and energy engineering series, CRC Press LLC, 2003.

[183] S. R. Turns, Understanding NO_x formation in nonpremixed flames: Experiments and modeling, Progress in Energy and Combustion Science 21 (5) (1995) 361–385.

[184] S. R. Turns, An introduction to combustion : concepts and applications, McGraw-Hill series in mechanical engineering, 2nd ed., McGraw-Hill, Boston, 2000.

[185] S. R. Turns, R. V. Bandaru, Carbon monoxide emissions from turbulent nonpremixed jet flames, Combustion and Flame 94 (4) (1993) 462–468.

[186] S. R. Turns, F. H. Myhr, Oxides of nitrogen emissions from turbulent jet flames: Part I – Fuel effects and flame radiation, Combustion and Flame 87 (3-4) (1991) 319–335.

[187] S. R. Turns, F. H. Myhr, R. V. Bandaru, E. R. Maund, Oxides of nitrogen emissions from turbulent jet flames: Part II – Fuel dilution and partial premixing effects, Combustion and Flame 93 (3) (1993) 255–269.

[188] D. C. Vaz, J. P. Van Buijtenen, A. R. Borges, H. Spliethoff, On the stability range of a cylindrical combustor for operation in the FLOX regime, in: 2004 ASME Turbo Expo, Jun 14-17 2004, vol. 1 of Proceedings of the ASME Turbo Expo 2004, American Society of Mechanical Engineers, New York, United States, 2004, pp. 511–516.

[189] A. L. Verlaan, S. Orsino, N. Lallemant, R. Weber, Fluid flow and mixing in a furnace equipped with the low NO_x regenerative burner of Nippon Furnace Kogyo, Tech. Rep. IFRF Doc. No. F46/y/1, International Flame Research Foundation (1998).

[190] Y. D. Wang, Y. Huang, D. McIlveen-Wright, J. McMullan, N. Hewitt, P. Eames, S. Rezvani, A techno-economic analysis of the application of continuous staged-combustion and flameless oxidation to the combustor design in gas turbines, Fuel Processing Technology 87 (8) (2006) 727–736.

[191] R. Weber, Scaling characteristics of aerodynamics, heat transfer, and pollutant emissions in industrial flames, Proceedings of the Combustion Institute 26 (1996) 3343–3354.

[192] R. Weber, J. F. Driscoll, W. J. A. Dahm, R. Waibel, Scaling characteristics of the aerodynamics and low-NO_x properties of industrial natural gas burners. SCALING 400-STUDY. Part I: Test Plan., Tech. Rep. IFRF Doc. No F40/y/8 and GRI-93/0227, International Flame Research Foundation (1993).

[193] R. Weber, S. Orsino, N. Lallemant, A. Verlaan, Combustion of natural gas with high-temperature air and large quantities of flue gas, Proceedings of the Combustion Institute 28 (2000) 1315–1321.

[194] R. Weber, A. L. Verlaan, S. Orsino, N. Lallemant, On emerging furnace design methodology that provides substantial energy savings and drastic reductions in CO_2, CO and NO_x emissions, Journal of the Institute of Energy 72 (1999) 77–83.

[195] F. Weinberg, Heat-recirculating burners: Principles and some recent developments, Combustion Science and Technology 121 (1) (1996) 3–22.

[196] C. K. Westbrook, F. L. Dryer, Chemical kinetic modeling of hydrocarbon combustion, Progress in Energy and Combustion Science 10 (1) (1984) 1–57.

[197] D. C. Wilcox, Turbulence modeling for CFD, 2nd ed., DCW Industries, La Canada, Calif., 1998.

[198] J. Wünning, Method or apparatus for combusting fuel in a combustion chamber (Oct. 13 1992).

[199] J. Wünning, J. Wünning, Flameless oxidation to reduce thermal NO-formation, Progress in Energy and Combustion Science 23 (12) (1997) 81–84.

[200] W. Yang, W. Blasiak, High temperature air combustion in heat treatment furnace, in: Proceedings of High Temperature Air Combustion—The Quest for Zero Emissions in Industrial Furnaces, Stockholm, Sweden, 2003, pp. 21–34.

[201] W. Yang, W. Blasiak, Mathematical modelling of NO emissions from high-temperature air combustion with nitrous oxide mechanism, Fuel Processing Technology 86 (9) (2005) 943–957.

[202] W. Yang, W. Blasiak, Numerical study of fuel temperature influence on single gas jet combustion in highly preheated and oxygen deficient air, Energy 30 (2-4) (2005) 385–398.

[203] W. J. Yanta, R. A. Smith, Measurements of turbulence-transport properties with a laser Doppler velocimeter, in: AIAA 11th Aerospace Sciences

Meeting, No. 73-169, American Institute of Aeronautics and Astronautics, 1973.

[204] R. A. Yetter, F. L. Dryer, H. Rabitz, A comprehensive reaction-mechanism for carbon monoxide hydrogen oxygen kinetics, Combustion Science and Technology 79 (1-3) (1991) 97–128.

[205] M. G. Zabetakis, Flammability characteristics of combustible gases and vapors, Tech. Rep. Bulletin 627, US Bureau of Mines (1965).

[206] J. Zeldovich, The oxidation of nitrogen in combustion and explosions, Acta Physiochimica U.R.S.S. XXI (4).

[207] H. Zhang, G. Yue, J. Lu, Z. Jia, J. Mao, T. Fujimori, T. Suko, T. Kiga, Development of high temperature air combustion technology in pulverized fossil fuel fired boilers, Proceedings of the Combustion Institute 31 (2) (2007) 2779–2785.

Appendix A MILD Modelling Summary

Table A.1: MILD combustion modelling summary

Author(s)	Year	Exp. data	Burner configuration	Fuel	Software package	Turbulence model	Combustion model	Kinetic mechanism	Radiation model	NO_x model	Comments
de Joannon et al. [45]	2000	–	–	CH_4	Chemkin	–	PSR	Warnatz (40 species + 170 reactions)	–	–	Their numerical analysis with an O_2 content of 5% in the reactant mixture showed that MILD combustion can be represented by a two-stage oxidation process, in which the first stage occurs in rich diluted conditions, that involves species such as CO and H_2.
Fleck et al. [61]	2000	[171, 61]	CGRI	320 kW CH_4	TASCflow	standard $k-\epsilon$	ED	global two-step	optically dense gas	–	Predictions of temperature, velocities and major species depart from measured values. The results suggest that reactions close to the burner exit are controlled by turbulent mixing.
Ishii et al. [95]	2000	–	Regenerative slab reheat furnace with four burners	840 kW / burner NG	Fluent	standard $k-\epsilon$	ξ / β−PDF	15 species with equilibrium	–	Post-processing thermal, prompt and reburn	Only NO_x emissions at the exhaust were used for validation. Turbulence and super-equilibrium O atoms had a strong influence on the predictions of NO. While prompt-NO levels were not reported, reburning was found to be negligible.
Coelho et al. [32]	2001	[154, 147]	FLOX® (REKU-MAT)	5.4 kW CH_4	Fluent 4.8 + PIPES	standard $k-\epsilon$	EPFM	ITM-RWTH (49 species + 547 reactions)	Fluent: DTM PIPES: DO	Post-processing unsteady EPFM	Discrepancies for mean and RMS velocities. Underprediction of mean residence times close to the burner exit. NO_x was one order of magnitude lower than experiments at exhaust.
Orsino et al. [146], Mancini et al. [123]	2001, 2002	[189, 194, 193]	NFK-HRS with a pre-combustor chamber	580 kW NG	IFRF solver, Fluent 5.4	standard $k-\epsilon$	EBU, EDC, ξ / β−PDF	global two-step, 11 species with equilibrium, 13 species with equilibrium	IFRF: DTM, Fluent: DO	Post-processing thermal, prompt and reburn	Equilibrium models did not capture flame propagation in the fuel jet region. Nonetheless, major species profiles were well predicted and NO_x at the exhaust agreed with experiments. Thermal-NO formation accounted for 95% of emissions, while reburn was negligible.

Table A.1: MILD combustion modelling summary (continued)

Author(s)	Year	Exp. data	Burner configuration	Fuel	Software package	Turbulence model	Combustion model	Kinetic mechanism	Radiation model	NO_x model	Comments
Choi & Katsuki [27]	2002	–	counter-flow laminar flat flame	CH_4	Chemkin	–	1D laminar flame calculations	GRI-2.11	–	NO_x chemistry included	The numerical study showed that NO destruction or reburn is possible in MILD conditions due to intense mixing of the reactants with flue gases.
Evrard et al. [57]	2002	[57]	FLOX® (REGE-MAT)	200 kW NG	Fluent 5.4	standard $k-\epsilon$ with standard wall functions	ξ / β−PDF, ED	15 species with equilibrium and global one-step	DO	Post-processing thermal and prompt	Both combustion models overpredict wall temperatures and hence radiative heat fluxes. Turbulence affected NO_x predictions, which were only qualitative, and the prompt-NO route was negligible.
Tabacco et al. [180]	2002	[180]	FLOX® (REKU-MAT)	40 kW CH_4	Fluent, Chemkin III	Realizable $k-\epsilon$	ξ / β−PDF, ED, PSR	equilibrium assumption, global one-step, and GRI-3.0	DO	Post-processing thermal, prompt, N_2O-intermediate and reburn	The equilibrium assumption is not suitable for the large ignition delays. NO_x predictions are sensitive to turbulent fluctuations and departed at least one order of magnitude from the experiments. A PSR study with detailed kinetics revealed that although thermal-NO still contributes significantly to NO formation, N_2O−intermediate is the main pathway.
Dally et al. [37]	2004	[37]	FLOX® (REKU-MAT)	7 kW CH_4, CH_4/N_2, CH_4/CO_2	Fluent + RIF solver	modified standard $k-\epsilon$ ($C_{\epsilon 1}=1.52$)	EPFM	detailed chemistry	–	NO_x chemistry included	A comparison between measured and predicted temperatures at the furnace centreline showed fair agreement for the pure methane case and fairly large discrepancies for the CO_2 and N_2 dilution cases. Contour plots revealed a shift of the stoichiometric mixture fraction to higher scalar dissipation regions when fuel was diluted with inert gases.

Table A.1: MILD combustion modelling summary (continued)

Author(s)	Year	Exp. data	Burner configuration	Fuel	Software package	Turbulence model	Combustion model	Kinetic mechanism	Radiation model	NO_x model	Comments
Hekkens [87, 88, 86]	2004	[64, 2]	NFK-HRS in the reverse-flow HEC furnace	950 kW NG	Fluent 6.1	standard $k-\epsilon$ with standard wall functions	ξ / β−PDF, modified ED ($A = 0.6$, $B = 10^{23}$), EDC	equilibrium assumption, laminar flamelet concept, global four-step	DO	–	Axial velocities were consistently over-predicted for the air jet and under-predicted for the fuel jet in the near burner region for all combustion models. In general, temperatures were over-predicted with fairly large discrepancies in the reaction zone, where the weak fuel jet entrains the strong air jet. The equilibrium assumption is not suitable to represent the initial fuel jet propagation.
Park et al. [150]	2004	–	counter-flow diffusion flame	H_2-Air diluted with steam	Chemkin	–	1D laminar flame calculations	GRI-3.0	optically-thin approxi-mation	NO_x chemistry included	Steam was numerically added to the air stream in mole fractions from 0.3 - 0.85. The added H_2O caused a significant increase in OH radicals, but as expected, thermal-NO formation decreases.
de Joannon et al. [44]	2004	–	jet stirred flow reactor	$CH_4/O_2/N_2$ mixture	Chemkin 3.6	–	transient PSR - AURORA	Warnatz (34 species + 164 reactions), Battin-Leclerc & Barbe (64 species + 439 reactions)	–	–	The dynamic behaviour of CH_4 oxidation was characterised with both measurements and modelling at a temperature range from 1000 K to 1300 K for a variety of equivalence ratios in PSR conditions . The cyclic oscillations were classified according to inlet temperatures, C/O ratios and residence times. It was reported that the CH_3 recombination path is the major mechanism controlling the temperature oscillations. The effect of heat losses was not included.

Table A.1: MILD combustion modelling summary (continued)

Author(s)	Year	Exp. data	Burner configuration	Fuel	Software package	Turbulence model	Combustion model	Kinetic mechanism	Radiation model	NO_x model	Comments
Christo & Dally [31], Christo et al. [29, 30]	2004, 2005, 2007	[39, 38]	Jet in Hot Coflow (JHC)	80% CH_4 + 20% H_2 by mass	Fluent 6.2	modified standard $k-\epsilon$ ($C_{\epsilon 1} = 1.6$)	EDC, TPDF + EMST	Smooke, GRI-3.0 without NO reactions, ARM-19	DO	–	In general, the EDC model with detailed kinetic mechanisms (e.g. GRI 3.0) yielded more accurate predictions than the TPDF model for conditions representative of MILD combustion, i.e. axial distance from the jet exit lower than ≈100 mm and O_2 levels in the coflow lower than 6%. At downstream locations, where the surrounding air mixes with the jet and coflow causing localised extinction, the TPDF model provided the best agreement with the experiments regardless of the kinetic mechanism used. Although turbulent mixing was accurately predicted, neither models captured the location for flame stabilisation.
Yang & Blasiak [201]	2005	[200]	HiTAC burner	200 kW LPG	STAR-CD	standard $k-\epsilon$	FRED	global five-step	DTM	Post-processing thermal, prompt, N_2O-intermediate and reburn	A comparison with NO_x emission measurements showed that NO predictions can be significantly improved when the N_2O-intermediate pathway is considered for excess air ratios (λ) less than 15%. NO_x emissions are overpredicted by a factor of two for $\lambda = 25\%$ due to the higher temperatures, which trigger the thermal-NO route. To decrease the discrepancies at high temperatures, the deactivation of the N_2O mechanism for temperatures above 1850 K was proposed.

Table A.1: MILD combustion modelling summary (continued)

Author(s)	Year	Exp. data	Burner configuration	Fuel	Software package	Turbulence model	Combustion model	Kinetic mechanism	Radiation model	NO_x model	Comments
Gkagkas et al. [68]	2005	[21]	Cabra burner	H_2	joint scalar PDF solver	modified standard $k-\epsilon$ ($C_{\epsilon 2}=1.8$)	TPDF + modified Curl	Li et al. [112]	–	–	A low temperature pre-ignition region was characterised by peak values of H_2O_2 and HO_2, while high concentrations of O, H, and OH radicals were an indication of autoignition. The modelling results showed that the TPDF approach was able to predict the ignition phenomena for diluted conditions similar to MILD combustion.
Christo & Dally [28]	2005	[39, 38]	Jet in Hot Coflow (JHC)	80% CH_4 + 20% H_2 by mass	Fluent 6.2	standard $k-\epsilon$, RNG $k-\epsilon$, Realizable $k-\epsilon$, modified standard $k-\epsilon$ ($C_{\epsilon 1}=1.6$)	laminar flamelet, ξ/β−PDF, FRED, EDC	Three-step global, Smooke, GRI-3.0 without NO reactions	DO	–	The modified $k-\epsilon$ provided the best agreement. Conserved scalar type models are inadequate for MILD conditions. For better accuracy detailed kinetic mechanisms must be used and differential diffusion effects should always be included.
Kim et al. [100]	2005	[39, 38]	Jet in Hot Coflow (JHC)	80% CH_4 + 20% H_2 by mass	VODE solver with a laminar flamelet library	modified standard $k-\epsilon$ ($C_{\epsilon 1}=1.5$)	CMC	GRI-2.11	–	NO_x chemistry included	A single mixture fraction parameter was used to define a three-stream mixing problem. Model predicted major species and temperatures reasonably well. Good predictions of NO profiles.
Awosope & Lockwood [10]	2005	[199, 189, 111]	FLOX®, NFK-HRS with a pre-combustor chamber, TECHNION afterburner	CH_4, 50% C_3H_8 + 50% C_4H_{10} by volume	FAFNIR-3D	standard $k-\epsilon$	ξ/β−PDF, laminar flamelet	CH_4: Warnatz (28 species + 72 reactions), C_3H_8 + C_4H_{10}: Marinov [124] (36 species + 200 reactions)	noneq. diffusion	Post-processing thermal, and prompt	Local extinction was important when high momentum jets are used to induce internal flue gas recirculation for strong dilution. Only qualitative agreement was found for CO profiles. The prompt-NO route was found to be negligible.

Table A.1: MILD combustion modelling summary (continued)

Author(s)	Year	Exp. data	Burner configuration	Fuel	Software package	Turbulence model	Combustion model	Kinetic mechanism	Radiation model	NO_x model	Comments
Yang & Blasiak [202]	2005	–	Single fuel jet in a oxygen deficient high temperature cross-flow	0.5 kW C_3H_8	STAR-CD	RNG $k-\epsilon$	ED, modified ED ($A=1$, $B=0.5$) ($A=2$, $B=0.5$), ξ/β–PDF	global three-step, 11 species with equilibrium	DTM	Post-processing thermal, and prompt	The empirical constant A in the ED model was changed to slow combustion rates. The numerical analysis showed an increased reaction zone volume for 5% O_2 levels in the cross-flow air. The low oxygen concentrations decreased NO formation, despite the fact that the fuel residence time in the reaction zone increased.
Nicolle & Dagaut [141]	2006	–	–	CH_4	Chemkin 4.0	–	PSR, PaSR, PFR - Senkin	skeletal mechanism derived from [35] (95 species + 265 reactions), GRI-3.0, Konnov-0.5	–	NO_x chemistry included	The kinetic modelling analysis showed the sequential nature of the nitrogen chemistry at constant temperature in MILD conditions. During the ignition period, the NO–HCN conversion reactions are particularly active. The NO-reburning mechanism is mainly related to the fuel-ignition chemistry and depends on the equivalence ratio and mixing times. In the post-ignition period, the thermal-NO and N_2O-intermediate pathways increase in importance.
Sabia et al. [163]	2007	[44, 42]	jet stirred flow reactor	CH_4–H_2/ O_2/N_2 mixture	Chemkin 3.7	–	transient PSR - AURORA	(34 species + 164 reactions), (99 species + 734 reactions)	–	–	The effect of hydrogen addition on methane combustion was studied for MILD conditions. As expected, the addition of H_2 in molar fractions from 0.25% to 0.9% caused an increase in reactivity and a reduction of instabilities related to thermokinetic temperature oscillations.
Galletti et al. [67]	2007	[67]	Enel radiant tube	13 kW CH_4	CFX 5.7	modified standard $k-\epsilon$ ($C_{\epsilon 1}=1.6$)	FRED	global one-step	DTM	Post-processing thermal and prompt	Only wall temperatures are available for validation. An axisymmetric model overestimated K_V in the burner by 15-20% when compared to a 3D model. Despite the difference, a regression equation for NO emissions as a function of K_V is proposed.

Table A.1: MILD combustion modelling summary (continued)

Author(s)	Year	Exp. data	Burner configuration	Fuel	Software package	Turbulence model	Combustion model	Kinetic mechanism	Radiation model	NO_x model	Comments
Dally & Peters [36]	2007	–	–	$CH_4/O_2/N_2$ mixture	Chemkin 4.1	–	transient PSR - AURORA	GRI 3.0, Smooke	–	–	The PSR calculations for CH_4 and C_2H_4 at a low temperature range of 1000 K to 1300 K showed that temperature oscillations are independent of the inlet temperature. It was also found that oscillations are controlled by a radical scavenging mechanism followed by heat loss to the surroundings, rather than a recombination channel.
Kumar et al. [107]	2007	[105, 106]	High intensity low-emission burner	3 kW and 150 kW C_3H_8	CFX 5.6	standard $k-\epsilon$	EDC	skeletal mechanism	–	–	A flame extinction criteria was initially proposed to predict the lift-off height of CH_4, C_3H_8 and H_2 flames and then used capture the flame propagation in a MILD burner. Essentially, if $Da < 1$ then the average reaction rate was set to zero in the EDC model. Temperatures were overpredicted by $\approx$ 200 K throughout the furnace for the 3 kW case. The overprediction of O_2 concentrations at a downstream location, and particularly on the fuel jet region, implies that the reaction zone structure is not fully captured. No velocity data was available for validation.
Mancini et al. [122]	2007	[189, 194, 193]	NFK-HRS with a pre-combustor chamber	580 kW NG	IFRF solver, Fluent 5.4, Chemkin 3.7	standard $k-\epsilon$, RNG	EBU, $\xi/\beta-$PDF, PSR network	global two-step, 13 species with equilibrium, & GRI-3.0	IFRF: DTM, Fluent: DO	Post-processing thermal, prompt and reburn	The failure of RANS models to predict the weak fuel jet structure is due to discrepancies in predicting entrainment. There is little combustion within the fuel jet, which means the temperature increase and the presence of NO is a result of entrainment.

Table A.1: MILD combustion modelling summary (continued)

Author(s)	Year	Exp. data	Burner configuration	Fuel	Software package	Turbulence model	Combustion model	Kinetic mechanism	Radiation model	NO_x model	Comments
Lupant et al. [117]	2007	[57, 118, 117]	FLOX® (REGE-MAT)	200 kW NG	Fluent 6.1	standard $k-\epsilon$ with standard wall functions	ED, FRED, modified ED ($A = 0.6$, $B = 10^{20}$), ξ/β−PDF	global one-step, global two-step, 15 species with equilibrium	DO	Post-processing thermal and prompt	Temperatures were largely overpredicted in the near burner region for all combustion models. Using the measured air inlet temperature as an input and modifying the empirical constants in the ED model resulted in a better agreement. However, the location of the reaction zone was not captured based on O_2 profiles and OH visualisation. Exhaust NO_x was on the same order of magnitude than in the experiments .
Duwig et al. [54]	2008	[54]	Flameless gas turbine combustor	460 kW C_3H_8	LES code + Cantera	LES	chemistry tabulated with PSR calculations	San Diego (46 species + 235 reactions)	–	–	The numerical results provided an insight into the unsteady aerodynamics of the flameless combustor. The analysis determined that the unburned gases entrained the same amount of combustion products before reaction, meaning a 0.5 global dilution rate.
Kim et al. [99]	2008	[189, 194, 193]	NFK-HRS with a pre-combustor chamber	580 kW NG	AIOLOS-3D	standard $k-\epsilon$	EDC	global three-step, global four-step	DO	Thermal, prompt, and reburn	A comparison of four different global reaction mechanisms for CH_4 showed fairly large discrepancies in the near burner region for temperature and major species. To improve the predictions a modified Jones and Lindstedt mechanism [97] was proposed. Although a better agreement was seen for CO and H_2, the global mechanism still did not capture the weak fuel jet structure. No information on the relative contribution of each NO formation pathway was presented.

Appendix B Temperature Correction

B.1 Methodology

The correction to the temperature measurements for radiation was determined from a steady-state energy balance on the thermocouple bead surface. The actual gas temperature (T_g) was determined from the measured temperature (T_{tcb}) and net radiation flux between diffuse-gray surfaces in an enclosure according to

$$T_g = T_{tcb} + \frac{A_{tcb}\epsilon_{tcb}\sum_{w=1}^{N}\sigma G_{1w}\left(T_{tcb}^4 - T_w^4\right)}{h}, \tag{B.1}$$

where A_{tcb} is the thermocouple bead surface area, ϵ_{tcb} is the thermocouple bead surface emissivity, N is the total number of surfaces (i.e. walls) in the enclosure, σ is the Stefan-Boltzmann constant, G_{1w} is the fraction of radiation emitted by the thermocouple bead that is incident on a particular wall surface w in the furnace enclosure and is absorbed [168], T_w is the surface temperature of wall w in the enclosure, and h is the convection coefficient. Catalytic and oxidation effects were neglected, as well as conductive heat transfer along the ceramic sheath.

The convective heat transfer coefficient, h, was calculated for a sphere from the expression [91];

$$Nu = \frac{hD_{tcb}}{k} = 2 + \left(0.4Re^{1/2} + 0.06Re^{2/3}\right)Pr^{0.4}\left(\frac{\mu}{\mu_s}\right)^{1/4} \tag{B.2}$$

$$\begin{bmatrix} 0.71 < Pr < 380 \\ 3.5 < Re < 7.6 \times 10^{-4} \\ 1.0 < \left(\frac{\mu}{\mu_s}\right) < 3.2 \end{bmatrix}$$

where D_{tcb} is the thermocouple bead diameter, Nu is the Nusselt number, Re is the Reynolds number, Pr is the Prandtl number, k is the thermal conductivity, and μ is the dynamic viscosity. Air was used to approximate furnace gas properties for determining the parameters of equation B.2. The air jet bulk velocity (U) was used to calculate the Reynolds number. All properties were evaluated at T_{tcb}, except μ_s, which was evaluated at the film temperature defined as

$$T_f = \frac{T_{tcb} + T_{air}}{2}\,. \tag{B.3}$$

The thermocouple bead diameter (D_{tcb}) was determined from an image obtained with an Olympus BX60MF microscope using a 5× magnification objective. The image was processed with an open source image manipulation program. Figure B.1 shows the original image and processed image used to determine D_{tcb}. First, the process involved converting the image to a grayscale and applying an edge detection and enhancement algorithm to sharpen the image and reveal the circumference of the bead. Then, a calibration disc with a 1 mm scale was used to find a pixel-to-length ratio for images taken at a 5× magnification and generate a marker. Finally, the average circumference of the bead (red circle) was compared to the marker size, resulting in $D_{tcb} \approx 1.2$ mm.

The G_{1w} correction factor was obtained for each probe position by matrix inversion from a system of equations (equation 6.37 of Ref. [168]) written in compact notation as

$$[G_{kw}] = m^{-1} f\,; \quad m = \delta_{kw} + (\epsilon_w - 1)F_{kw}\,; \quad f = \epsilon_w F_{kw}\,; \tag{B.4}$$

where $1 \leq k \leq 7$, ϵ_w is the emissivity for surface w, F_{kw} is the configuration or view factor between surface k and w of the enclosure, δ_{kw} is the Kronecker delta, defined as

$$\delta_{kw} = \begin{cases} 1, & k = w \\ 0, & k \neq w \end{cases} \tag{B.5}$$

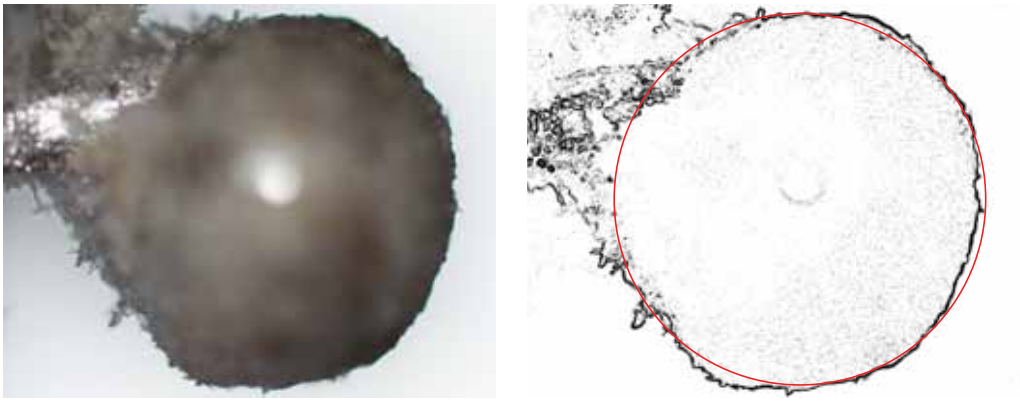

(a) original image **(b)** processed image

Figure B.1: Images used to determine the thermocouple bead diameter. The red circle represents the average circumference of the bead.

The bead emissivity used in the calculations was $\epsilon_1 = 0.22$, which is based on acceptable values of small diameter platinum-rhodium wires [83, 175], and the furnace wall emissivity was $\epsilon_2 = \epsilon_3 = \epsilon_4 = \epsilon_5 = \epsilon_6 = \epsilon_7 = 0.93$, which is the value provided by the manufacturer of the insulation material. This procedure always resulted in corrected temperatures lower than the adiabatic flame temperature.

B.2 Error Propagation

Some degree of uncertainty is associated with the methodology described in the previous section, since the parameters used in the calculations (equation B.1) are not precisely known. The errors introduced by each parameter will affect the resulting final gas temperature. A common approach to determine the total uncertainty (ΔT_g) is through an error propagation analysis. In this analysis, an estimated deviation is attributed to each parameter (Table B.1) and the propagation of errors is calculated from the following expression:

$$\Delta f = \sqrt{\sum_{i=1}^{n} \left(\frac{\partial f}{\partial a_i} \cdot \Delta a_i \right)^2} \tag{B.6}$$

$$\Delta T_g = \sqrt{\left(\frac{\partial T_g}{\partial T_w} \cdot \Delta T_w \right)^2 + \left(\frac{\partial T_g}{\partial \epsilon_{tcb}} \cdot \Delta \epsilon_{tcb} \right)^2 + \left(\frac{\partial T_g}{\partial D_{tcb}} \cdot \Delta D_{tcb} \right)^2 + \left(\frac{\partial T_g}{\partial U} \cdot \Delta U \right)^2}.$$

Table B.1: Estimated uncertainty of the parameters used to calculate the temperature correction

Parameter (a_i)	Unit	Δ
T_w	°C	±10%
ϵ_{tcb}	–	±15%
D_{tcb}	mm	±5%
U	m/s	±5%

The results of the error estimation procedure are shown in Table B.2, where δ represents the correction between raw and actual gas temperatures in absolute and relative terms.

Table B.2: Error estimates for in-furnace temperature data for the baseline operating conditions

TC position			$T_{air} = 25$°C			$T_{air} = 450$°C		
x (mm)	y (mm)	z (mm)	δ (°C)	δ (%)	ΔT_g (%)	δ (°C)	δ (%)	ΔT_g (%)
-100	0	42.5	-40.2	-3.3	1.3	-8.6	-0.7	1.2
-100	55	42.5	-39.2	-3.2	1.3	-13.4	-1.1	1.2
-100	110	42.5	-37.7	-3.1	1.3	-8.7	-0.7	1.2
-100	140	42.5	-30.4	-2.6	1.3	-1.2	-0.1	1.3
-100	0	142.5	-43.6	-3.6	1.2	-16.6	-1.3	1.1
-100	55	142.5	-40.8	-3.4	1.2	-16.2	-1.3	1.1
-100	110	142.5	-41.7	-3.4	1.2	-8.4	-0.7	1.2

continued on next page

Table B.2: Error estimates for in-furnace temperature data for the baseline operating conditions (continued)

TC position			$T_{air} = 25°C$			$T_{air} = 450°C$		
x (mm)	y (mm)	z (mm)	δ (°C)	δ (%)	ΔT_g (%)	δ (°C)	δ (%)	ΔT_g (%)
-100	140	142.5	-25.4	-2.2	1.3	-8.8	-0.7	1.2
-100	0	242.5	-31.8	-2.7	1.3	4.4	0.4	1.4
-100	55	242.5	-37.2	-3.1	1.3	-6.7	-0.5	1.2
-100	110	242.5	-43.0	-3.5	1.2	-12.0	-1.0	1.2
-100	140	242.5	-23.1	-2.0	1.4	5.3	0.5	1.4
-100	0	342.5	-16.2	-1.4	1.4	3.3	0.3	1.3
-100	55	342.5	-31.8	-2.7	1.3	-7.3	-0.6	1.2
-100	110	342.5	-41.5	-3.4	1.2	-15.0	-1.2	1.1
-100	140	342.5	-17.5	-1.5	1.4	6.3	0.5	1.3
-100	0	442.5	-28.3	-2.4	1.3	-6.8	-0.6	1.2
-100	55	442.5	-33.6	-2.8	1.3	-9.0	-0.7	1.2
-100	110	442.5	-35.6	-3.0	1.3	-10.6	-0.9	1.1
-100	140	442.5	-15.5	-1.4	1.4	2.3	0.2	1.3
-100	0	542.5	-26.2	-2.2	1.3	-8.5	-0.7	1.2
-100	55	542.5	-27.7	-2.4	1.3	-10.2	-0.8	1.1
-100	110	542.5	-25.9	-2.2	1.3	-11.8	-0.9	1.1
-100	140	542.5	-18.8	-1.6	1.4	-5.5	-0.4	1.2
0	0	42.5	80.1	11.7	3.0	73.8	9.1	2.6
0	55	42.5	-33.4	-2.8	1.3	-11.5	-0.9	1.2
0	110	42.5	-1.4	-0.1	1.5	33.7	3.2	1.8
0	140	42.5	-17.2	-1.5	1.4	7.7	0.7	1.4
0	0	142.5	8.8	0.8	1.6	30.3	2.8	1.7
0	55	142.5	-22.7	-2.0	1.4	-20.7	-1.6	1.1
0	110	142.5	-39.7	-3.3	1.3	-11.8	-0.9	1.2
0	140	142.5	-26.4	-2.3	1.3	-2.8	-0.2	1.3
0	0	242.5	-22.9	-2.0	1.4	4.2	0.4	1.4
0	55	242.5	-21.3	-1.8	1.4	-15.7	-1.2	1.1

continued on next page

Table B.2: Error estimates for in-furnace temperature data for the baseline operating conditions (continued)

TC position			$T_{air} = 25°C$			$T_{air} = 450°C$		
x (mm)	y (mm)	z (mm)	δ (°C)	δ (%)	ΔT_g (%)	δ (°C)	δ (%)	ΔT_g (%)
0	110	242.5	-45.1	-3.7	1.2	-19.5	-1.5	1.1
0	140	242.5	-44.5	-3.6	1.2	-1.3	-0.1	1.3
0	0	342.5	-24.3	-2.1	1.3	-3.5	-0.3	1.2
0	55	342.5	-24.0	-2.1	1.4	-13.0	-1.0	1.1
0	110	342.5	-50.8	-4.1	1.2	-26.6	-2.0	1.0
0	140	342.5	-28.8	-2.4	1.3	-6.8	-0.6	1.2
0	0	442.5	-24.3	-2.1	1.3	-6.0	-0.5	1.2
0	55	442.5	-27.2	-2.3	1.3	-10.1	-0.8	1.1
0	110	442.5	-35.8	-3.0	1.3	-15.7	-1.2	1.1
0	140	442.5	-17.6	-1.5	1.4	-2.5	-0.2	1.2
0	0	542.5	-15.3	-1.3	1.3	-3.7	-0.3	1.2
0	55	542.5	-16.6	-1.5	1.3	-7.3	-0.6	1.2
0	110	542.5	-17.6	-1.5	1.3	-10.2	-0.8	1.1
0	140	542.5	-9.3	-0.8	1.4	-0.6	0	1.3
100	0	42.5	-41.6	-3.4	1.2	-15.4	-1.2	1.1
100	55	42.5	-38.2	-3.2	1.3	-13.5	-1.1	1.2
100	110	42.5	-39.4	-3.3	1.3	-14.6	-1.2	1.2
100	140	42.5	-27.4	-2.3	1.3	-2.7	-0.2	1.3
100	0	142.5	-51.8	-4.1	1.2	-15.9	-1.3	1.1
100	55	142.5	-49.1	-4.0	1.2	-22.5	-1.7	1.1
100	110	142.5	-51.3	-4.1	1.2	-21.8	-1.7	1.1
100	140	142.5	-29.8	-2.5	1.3	-6.5	-0.5	1.2
100	0	242.5	-44.0	-3.6	1.2	-22.8	-1.8	1.1
100	55	242.5	-50.6	-4.1	1.2	-24.2	-1.9	1.1
100	110	242.5	-49.9	-4.0	1.2	-20.3	-1.6	1.1
100	140	242.5	-29.4	-2.5	1.3	-4.7	-0.4	1.3
100	0	342.5	-30.4	-2.6	1.3	-13.2	-1.0	1.1

continued on next page

Table B.2: Error estimates for in-furnace temperature data for the baseline operating conditions (continued)

TC position			$T_{air} = 25°C$			$T_{air} = 450°C$		
x (mm)	y (mm)	z (mm)	δ (°C)	δ (%)	ΔT_g (%)	δ (°C)	δ (%)	ΔT_g (%)
100	55	342.5	-31.6	-2.7	1.3	-17.5	-1.4	1.1
100	110	342.5	-36.0	-3.0	1.3	-13.8	-1.1	1.1
100	140	342.5	-20.6	-1.8	1.4	-13.0	-1.0	1.1
100	0	442.5	-23.0	-2.0	1.4	-7.6	-0.6	1.2
100	55	442.5	-22.3	-1.9	1.4	-11.0	-0.9	1.1
100	110	442.5	-23.6	-2.0	1.4	-9.6	-0.8	1.1
100	140	442.5	-15.7	-1.4	1.4	1.7	0.1	1.3
100	0	542.5	-21.3	-1.8	1.3	-4.8	-0.4	1.2
100	55	542.5	-16.8	-1.5	1.3	-7.7	-0.6	1.2
100	110	542.5	-16.7	-1.5	1.3	-8.4	-0.7	1.2
100	140	542.5	-13.6	-1.2	1.4	-1.4	-0.1	1.2

Appendix C Control Logic

This is a simplified flowdiagram that illustrates the main steps involved in the logic integrated in the BMS that controls the MILD combustion burner system.

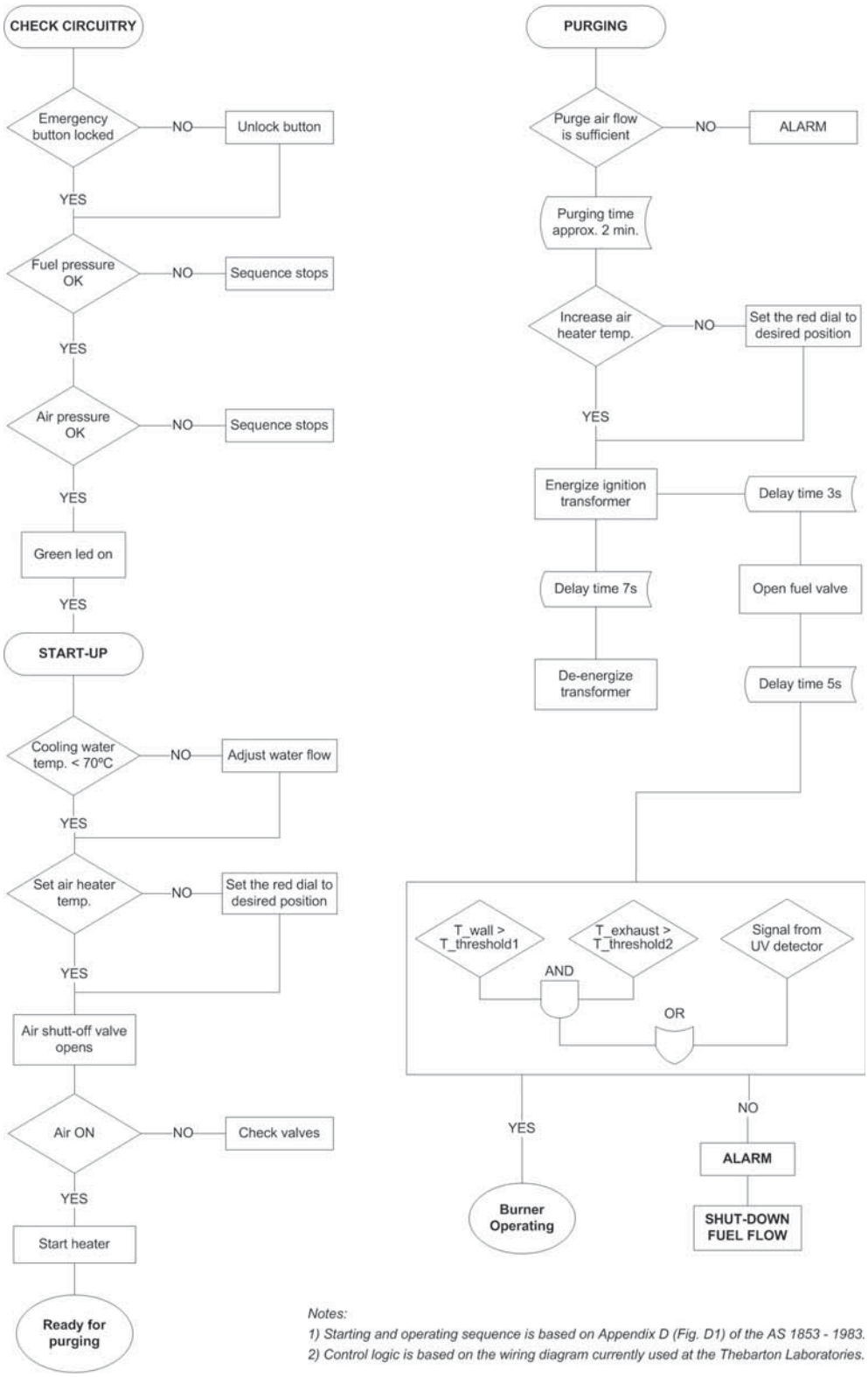

Figure C.1: Flowdiagram of the control logic integrated in the burner management system (BMS).

Appendix D Particle Size Distribution

This histogram shows the particle size distribution of the fused white alumina powder used to seed the central air jet for the LDA measurements. The particle size analysis was carried out by Pulver Technology Ltd., which is the company that supplied the seeding material.

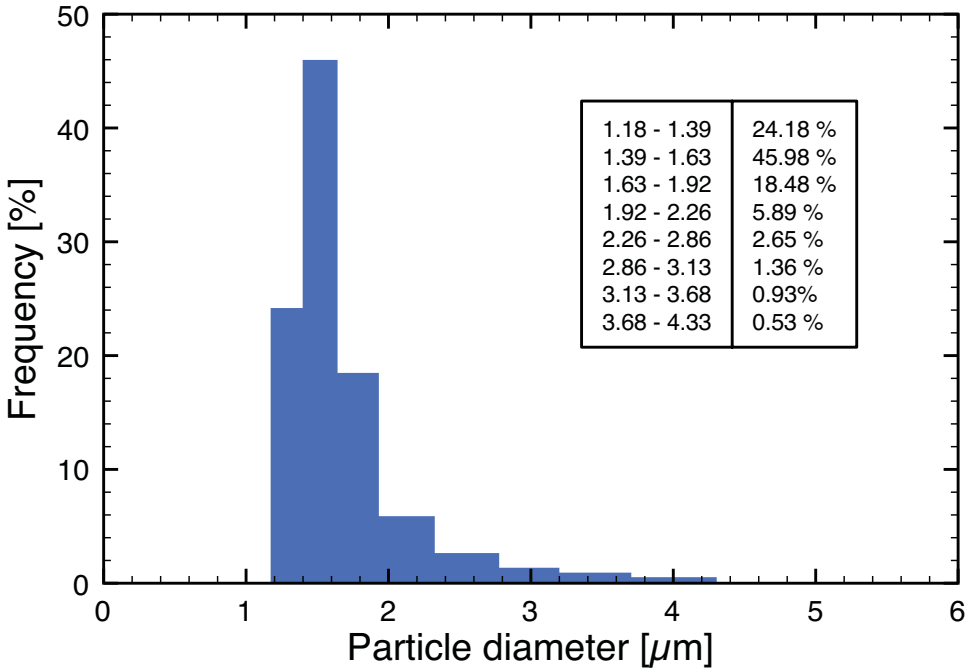

Figure D.1: Al_2O_3 particle size distribution. (*Source*: Pulver Technology Ltd.)

Appendix E Velocity for Nonreacting Isothermal Conditions

The results presented in Figures 7.1 through 7.4 are repeated here for convenience to show the comparison for the realizable $k - \epsilon$ turbulence model alone.

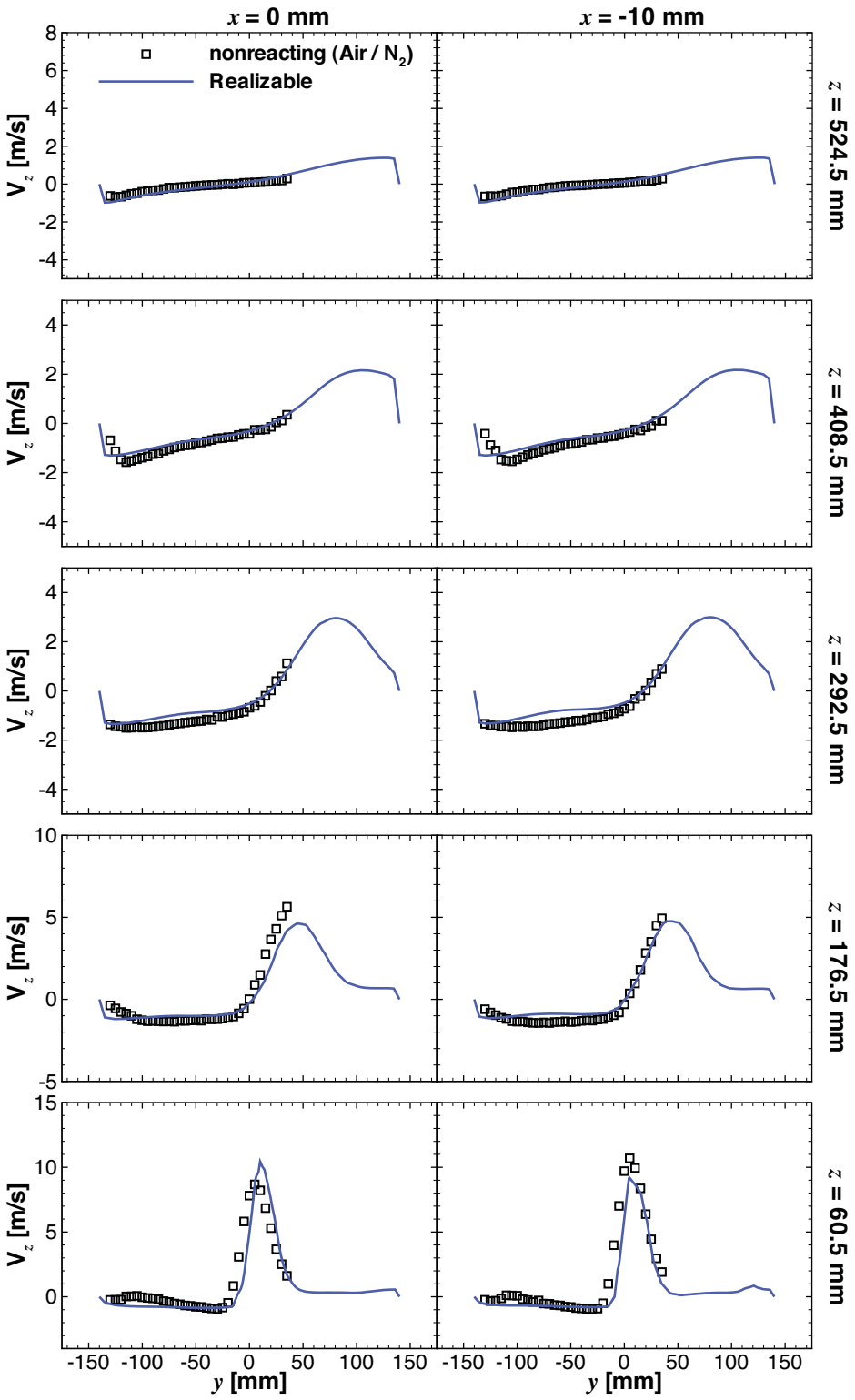

Figure E.1: Comparison of measured (open symbols) and predicted (blue lines) mean axial velocity (V_z) profiles across the $y-$axis for nonreacting conditions at $x = 0$ (left) and $x = -10$ (right) for the realizable $k - \epsilon$ turbulence model at various axial locations.

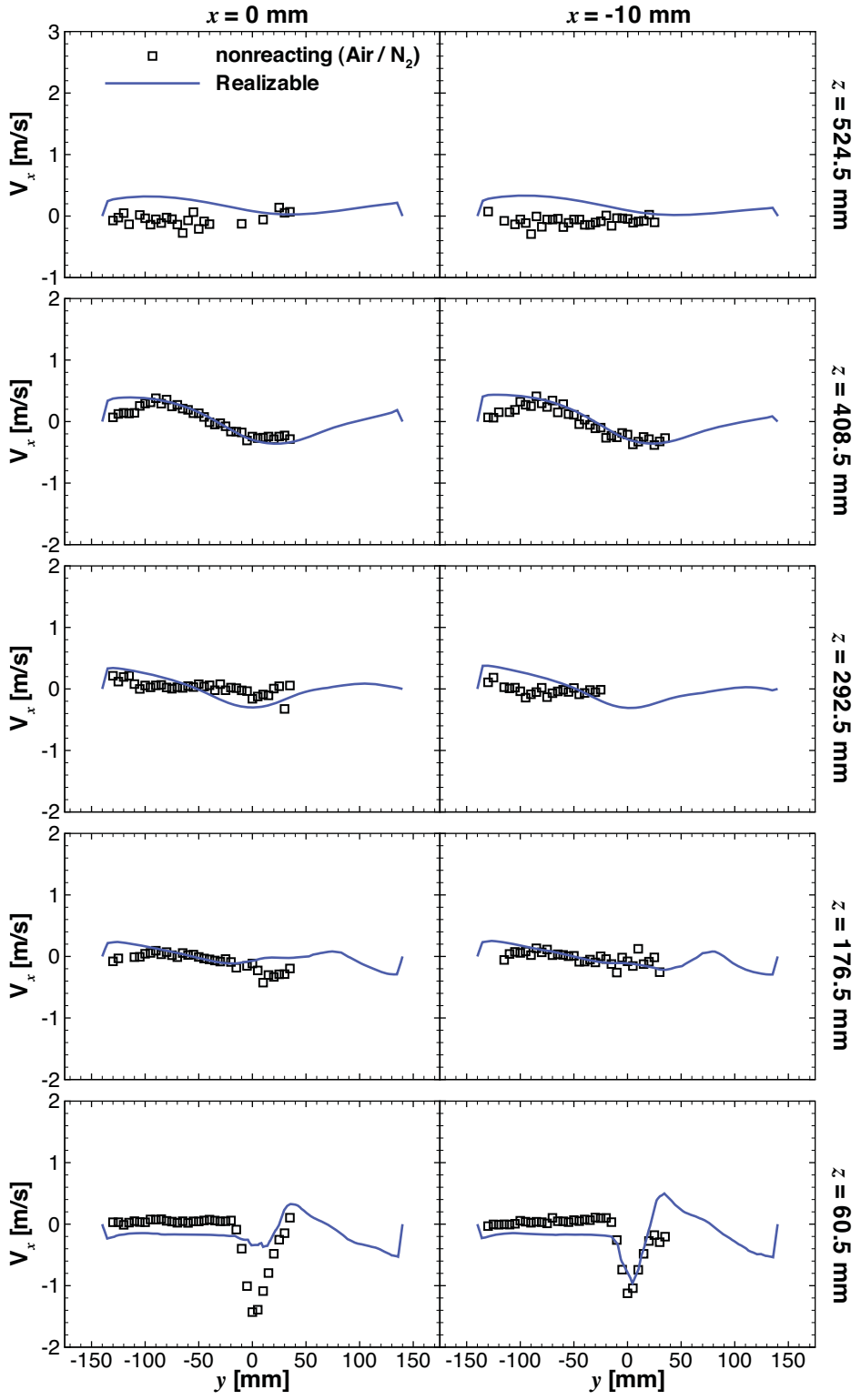

Figure E.2: Comparison of measured (open symbols) and predicted (blue lines) mean radial velocity (V_x) profiles across the $y-$axis for nonreacting conditions at $x = 0$ (left) and $x = -10$ (right) for the realizable $k - \epsilon$ turbulence model at various axial locations.

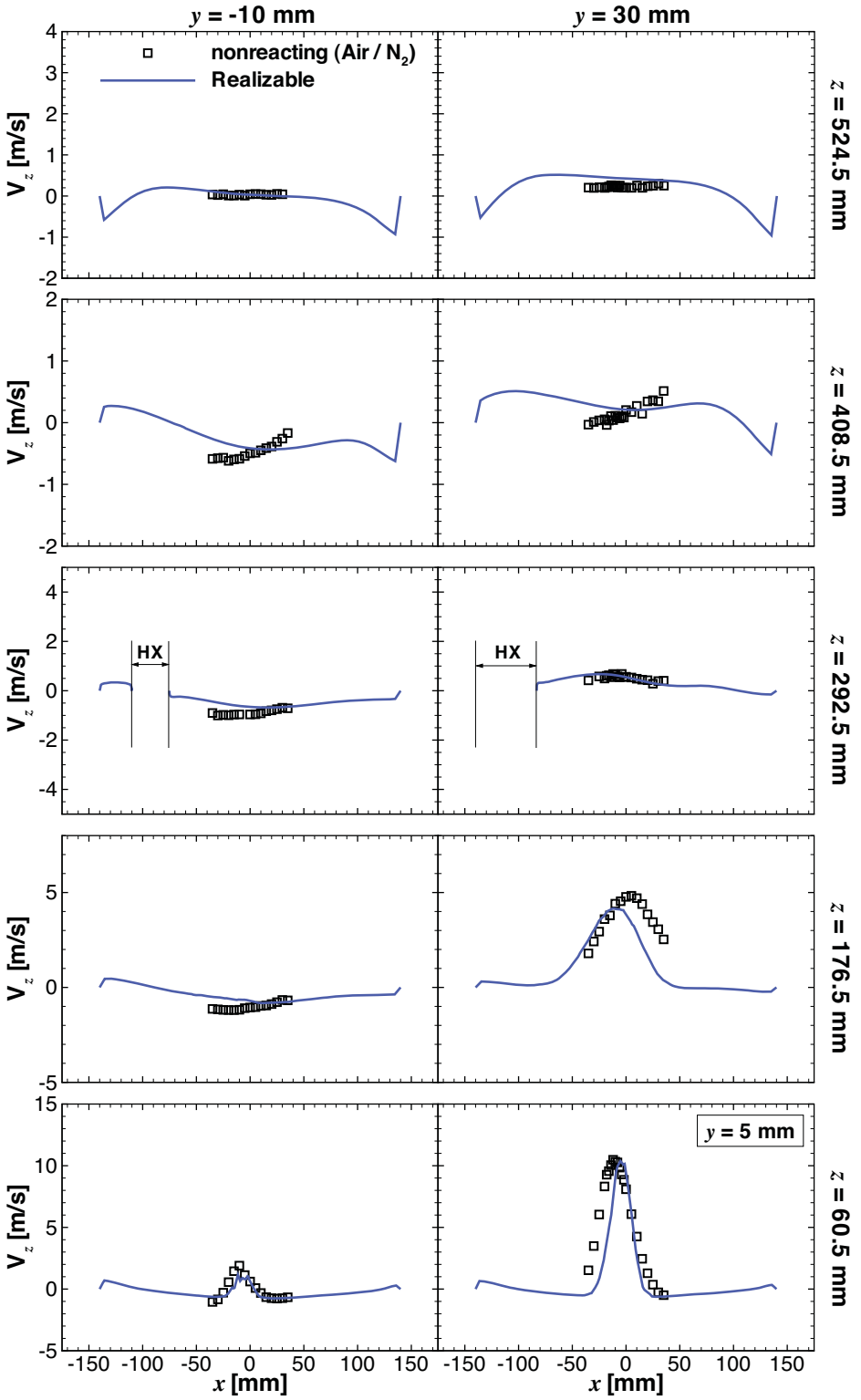

Figure E.3: Comparison of measured (open symbols) and predicted (blue lines) mean axial velocity (V_z) profiles across the $x-$axis for nonreacting conditions at $y = -10$ (left) and $y = 30$ (right) with the exception of $y = 5$ (lower right) for the realizable $k - \epsilon$ turbulence model at various axial locations.

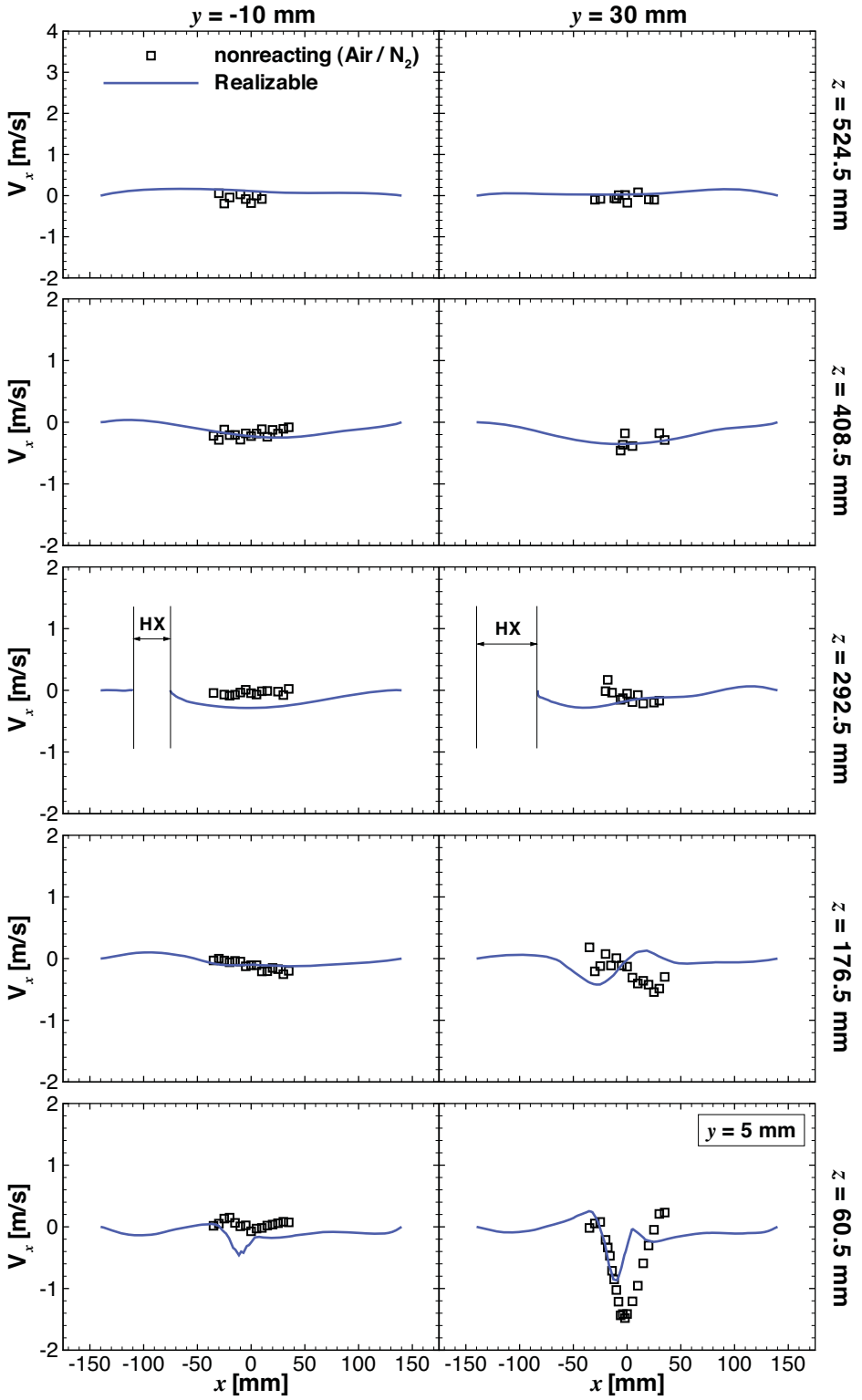

Figure E.4: Comparison of measured (open symbols) and predicted (blue lines) mean radial velocity (V_x) profiles across the $x-$axis for nonreacting conditions at $y = -10$ (left) and $y = 30$ (right) with the exception of $y = 5$ (lower right) for the realizable $k - \epsilon$ turbulence model at various axial locations.

Appendix F Compositional Struture Contours

It must be noted that the mole fraction contours of all species presented in this Appendix are displayed on a wet basis.

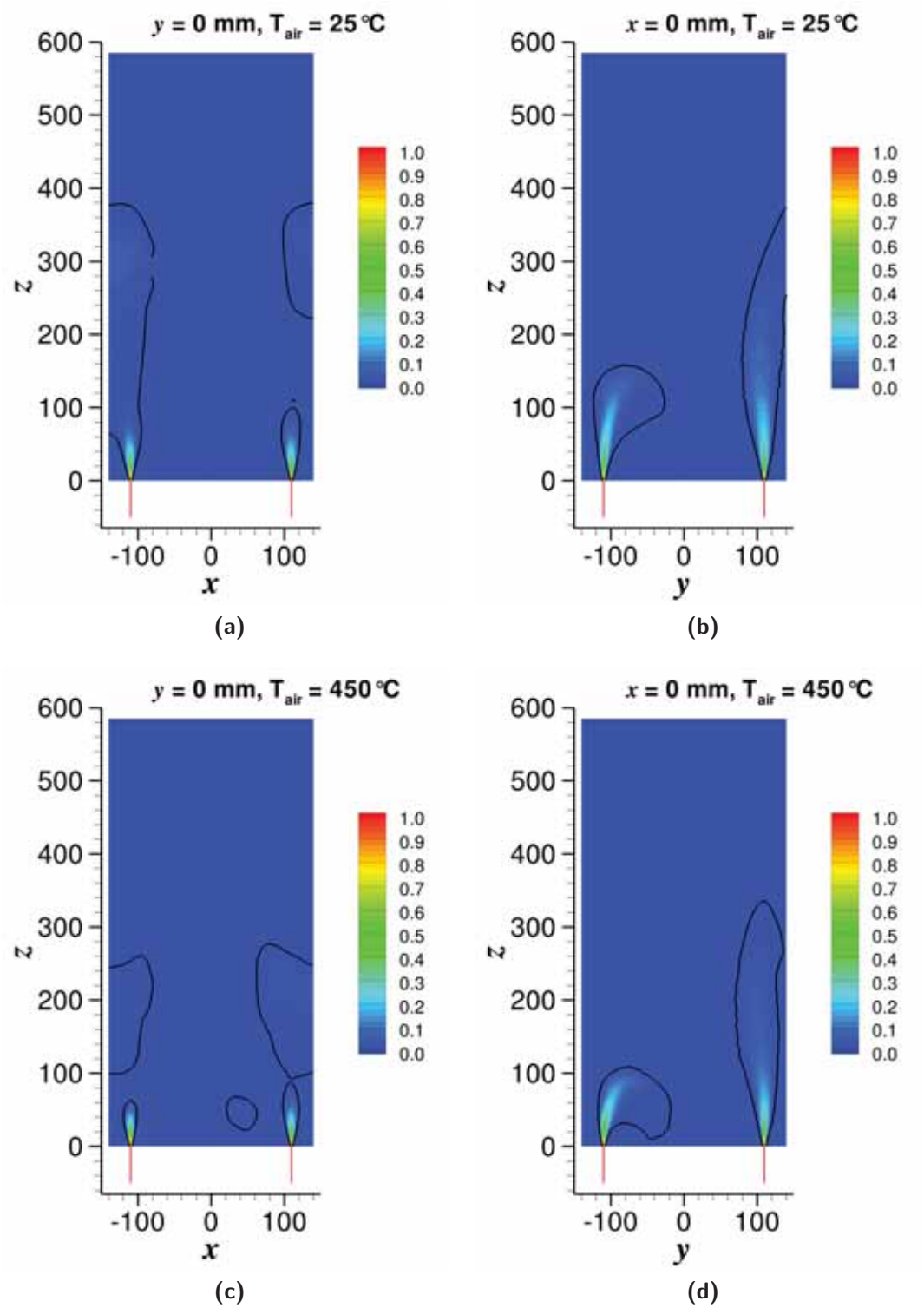

Figure F.1: Predicted CH_4 mole fraction contours with stoichiometric surface ($\xi_{st} = 0.0552$) overlaid for the baseline case, (a) and (b) without air preheat, $T_{air} = 25°C$, and (c) and (d) with air preheat, $T_{air} = 450°C$, for the EDC model with the Smooke mechanism at the $x - z$ and $y - z$ centreline planes.

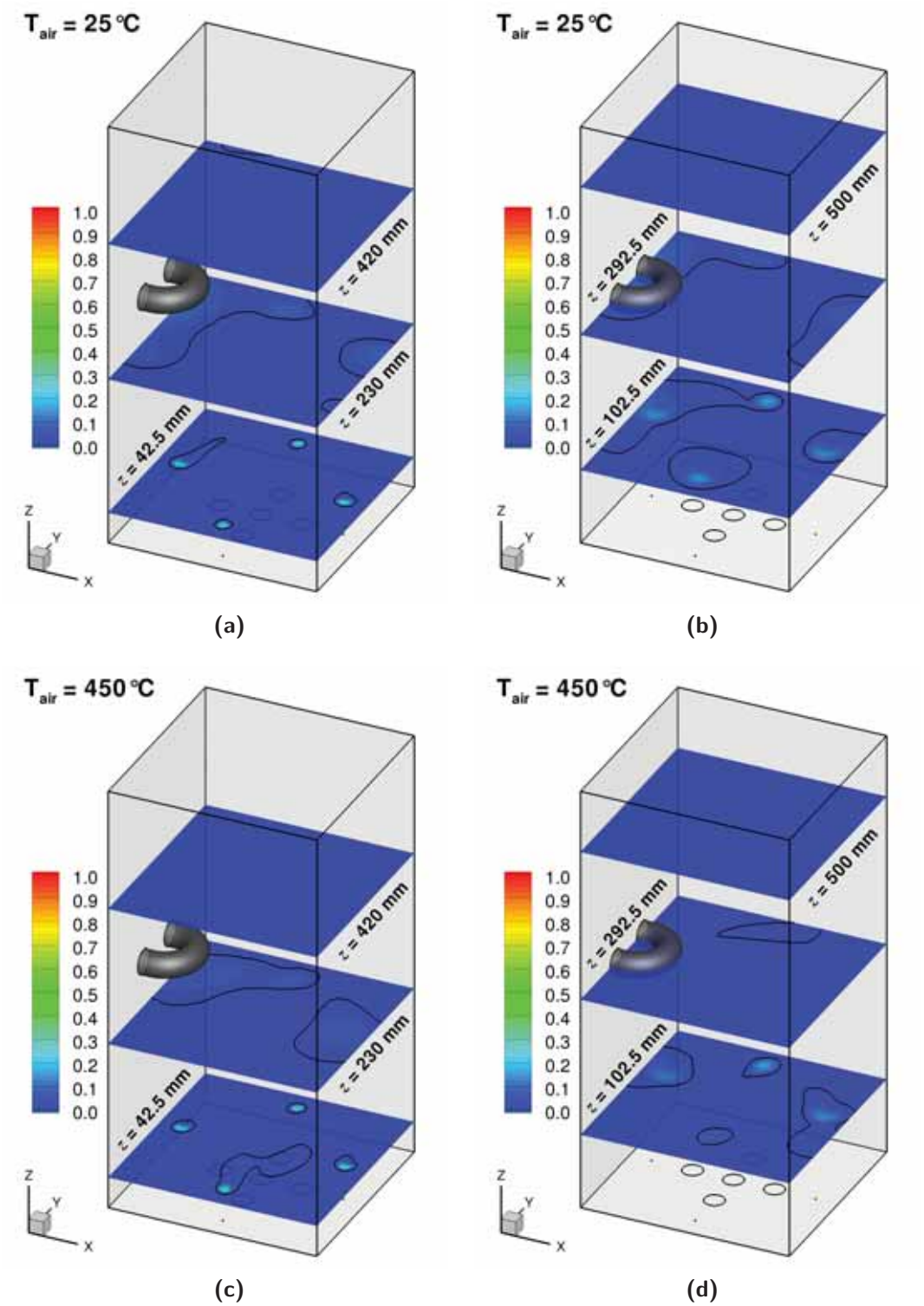

Figure F.2: Predicted CH_4 mole fraction contours with stoichiometric surface ($\xi_{st} = 0.0552$) overlaid for the baseline case, (a) and (b) without air preheat, $T_{air} = 25°C$, and (c) and (d) with air preheat, $T_{air} = 450°C$, for the EDC model with the Smooke mechanism at different $x - y$ planes.

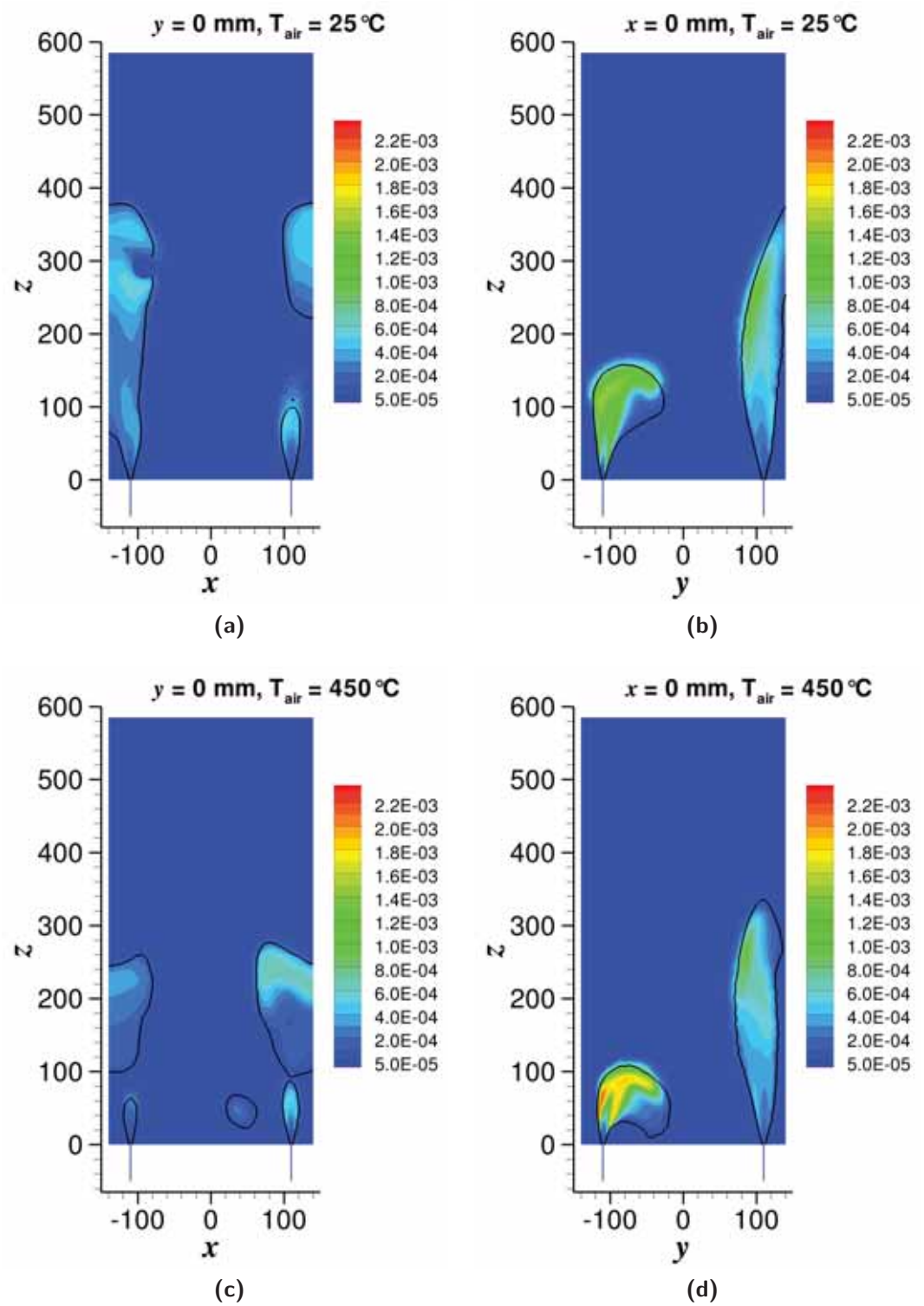

Figure F.3: Predicted CH_3 mole fraction contours with stoichiometric surface ($\xi_{st} = 0.0552$) overlaid for the baseline case, (a) and (b) without air preheat, $T_{air} = 25°C$, and (c) and (d) with air preheat, $T_{air} = 450°C$, for the EDC model with the Smooke mechanism at the $x - z$ and $y - z$ centreline planes.

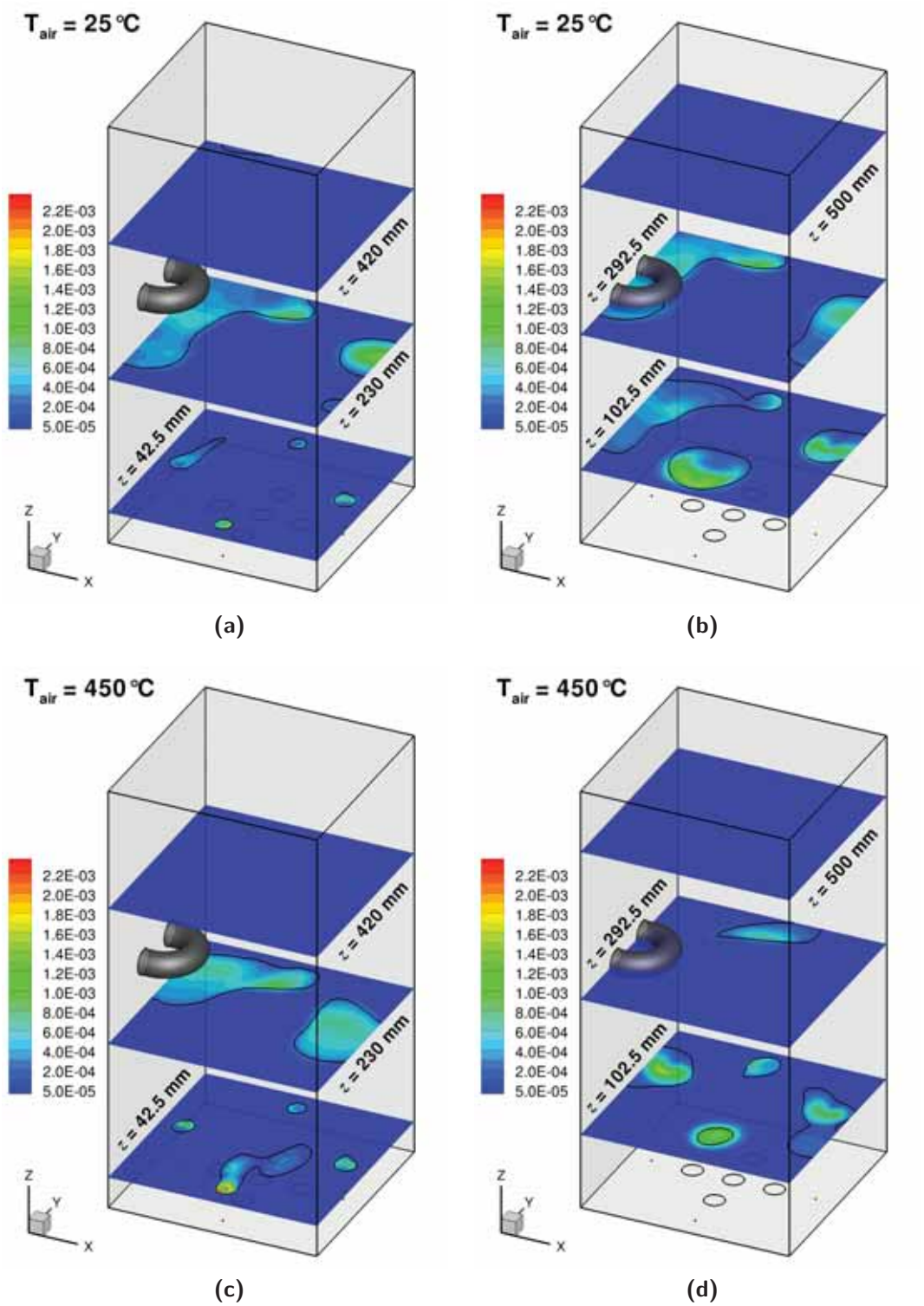

Figure F.4: Predicted CH_3 mole fraction contours with stoichiometric surface ($\xi_{st} = 0.0552$) overlaid for the baseline case, (a) and (b) without air preheat, $T_{air} = 25°C$, and (c) and (d) with air preheat, $T_{air} = 450°C$, for the EDC model with the Smooke mechanism at different $x - y$ planes.

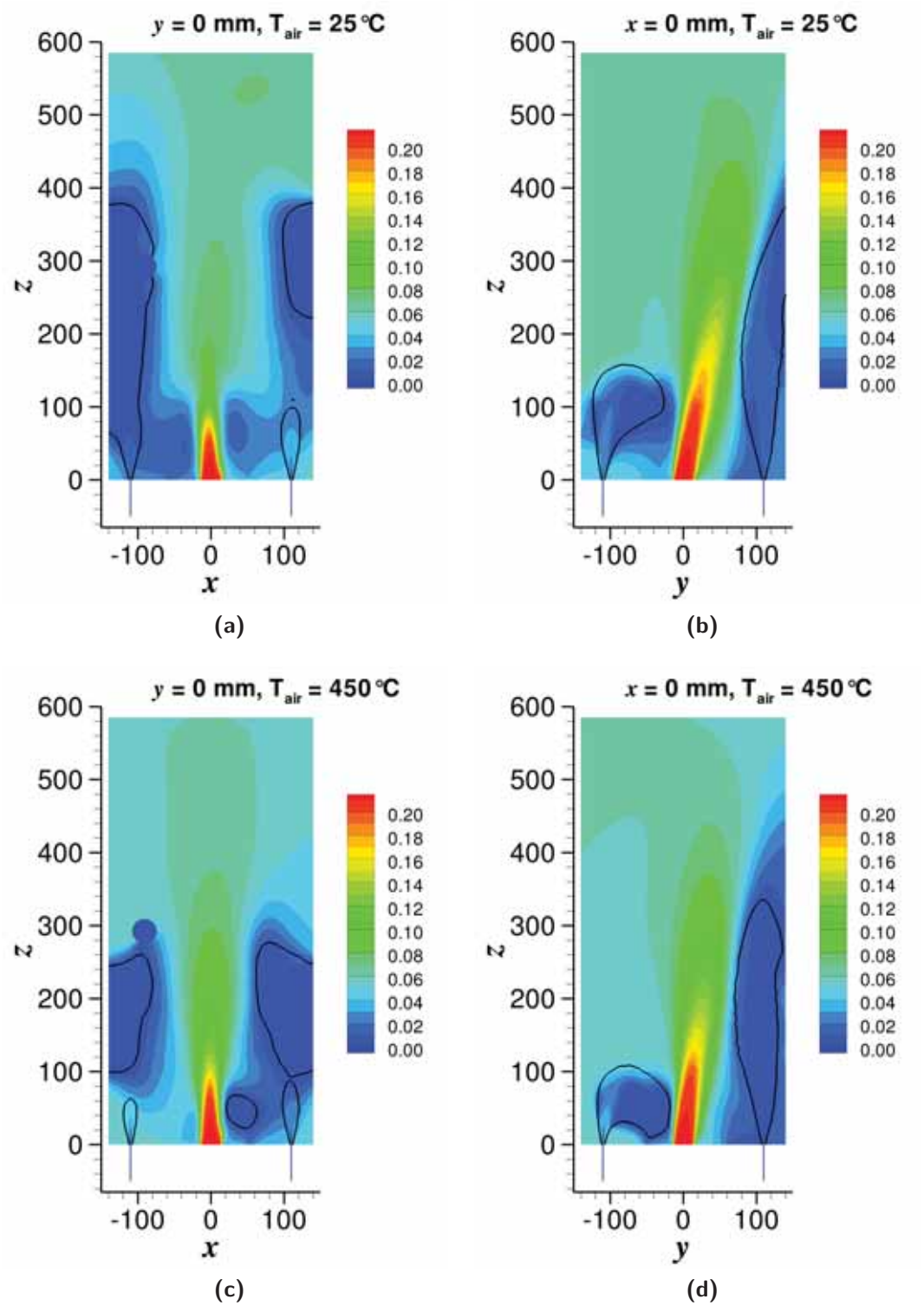

Figure F.5: Predicted O_2 mole fraction contours with stoichiometric surface ($\xi_{st} = 0.0552$) overlaid for the baseline case, (a) and (b) without air preheat, $T_{air} = 25°C$, and (c) and (d) with air preheat, $T_{air} = 450°C$, for the EDC model with the Smooke mechanism at the $x - z$ and $y - z$ centreline planes.

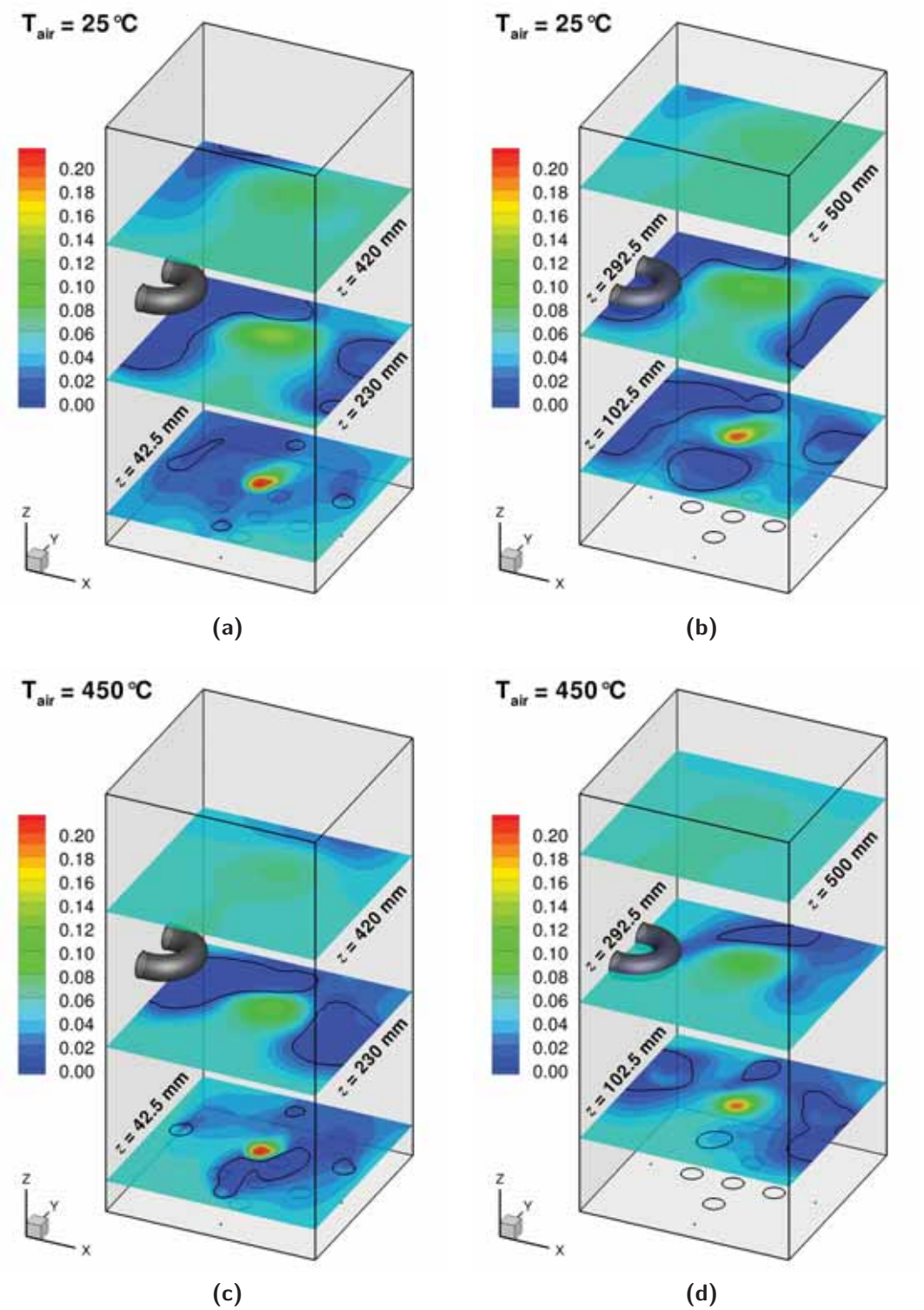

Figure F.6: Predicted O_2 mole fraction contours with stoichiometric surface ($\xi_{st} = 0.0552$) overlaid for the baseline case, (a) and (b) without air preheat, $T_{air} = 25°C$, and (c) and (d) with air preheat, $T_{air} = 450°C$, for the EDC model with the Smooke mechanism at different $x - y$ planes.

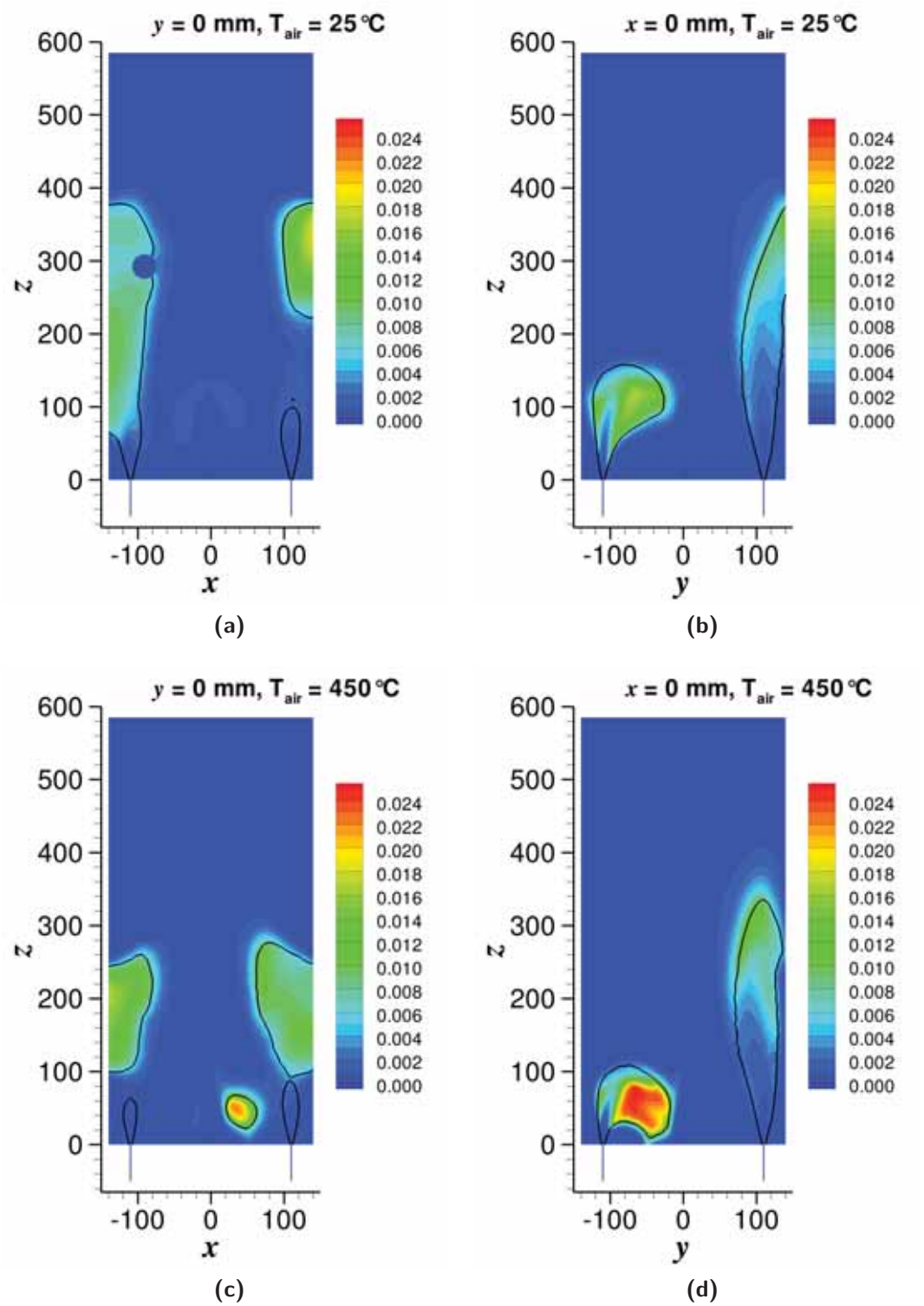

Figure F.7: Predicted CO mole fraction contours with stoichiometric surface ($\xi_{st} = 0.0552$) overlaid for the baseline case, (a) and (b) without air preheat, $T_{air} = 25°C$, and (c) and (d) with air preheat, $T_{air} = 450°C$, for the EDC model with the Smooke mechanism at the $x - z$ and $y - z$ centreline planes.

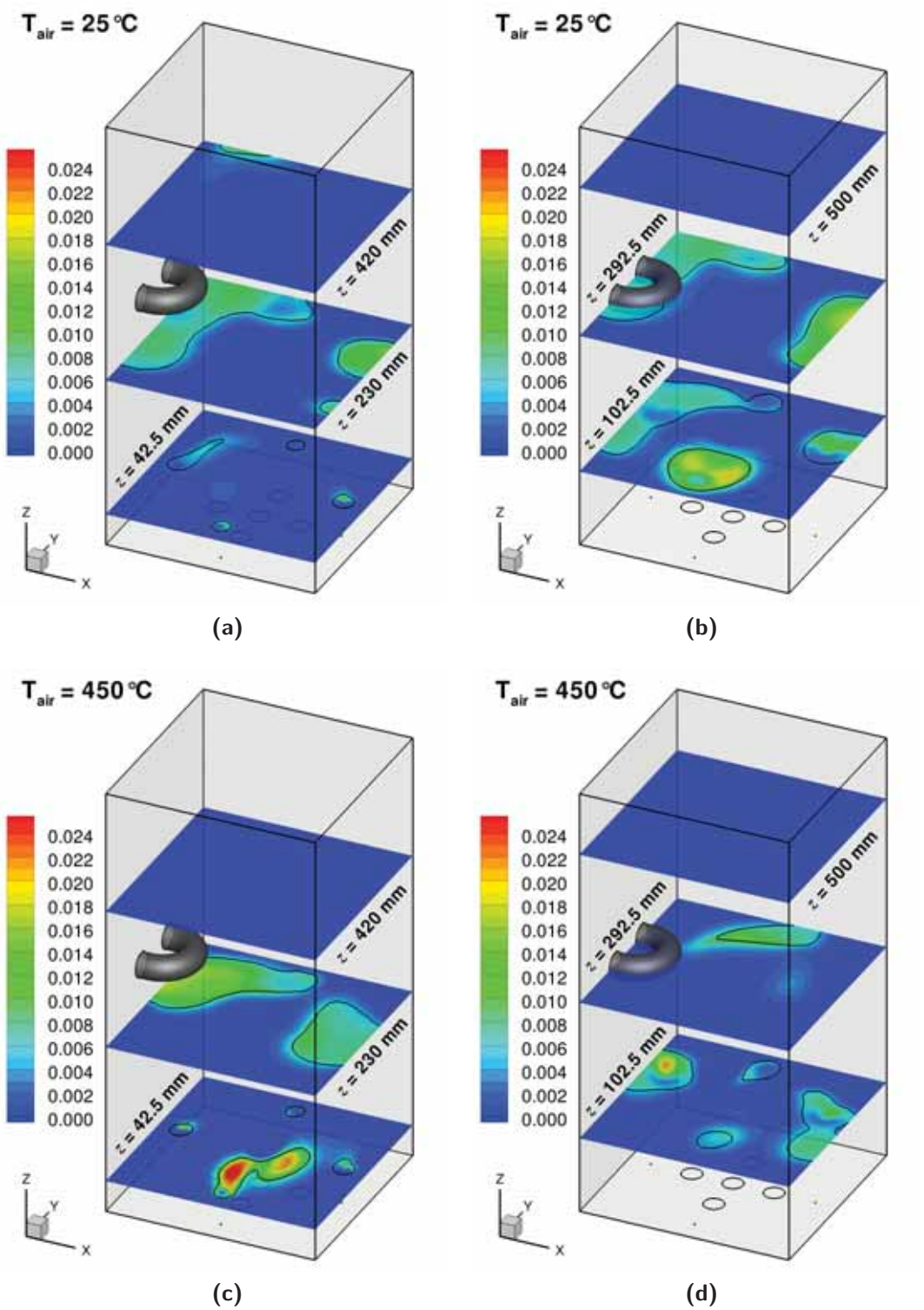

Figure F.8: Predicted CO mole fraction contours with stoichiometric surface ($\xi_{st} = 0.0552$) overlaid for the baseline case, (a) and (b) without air preheat, $T_{air} = 25°C$, and (c) and (d) with air preheat, $T_{air} = 450°C$, for the EDC model with the Smooke mechanism at different $x - y$ planes.

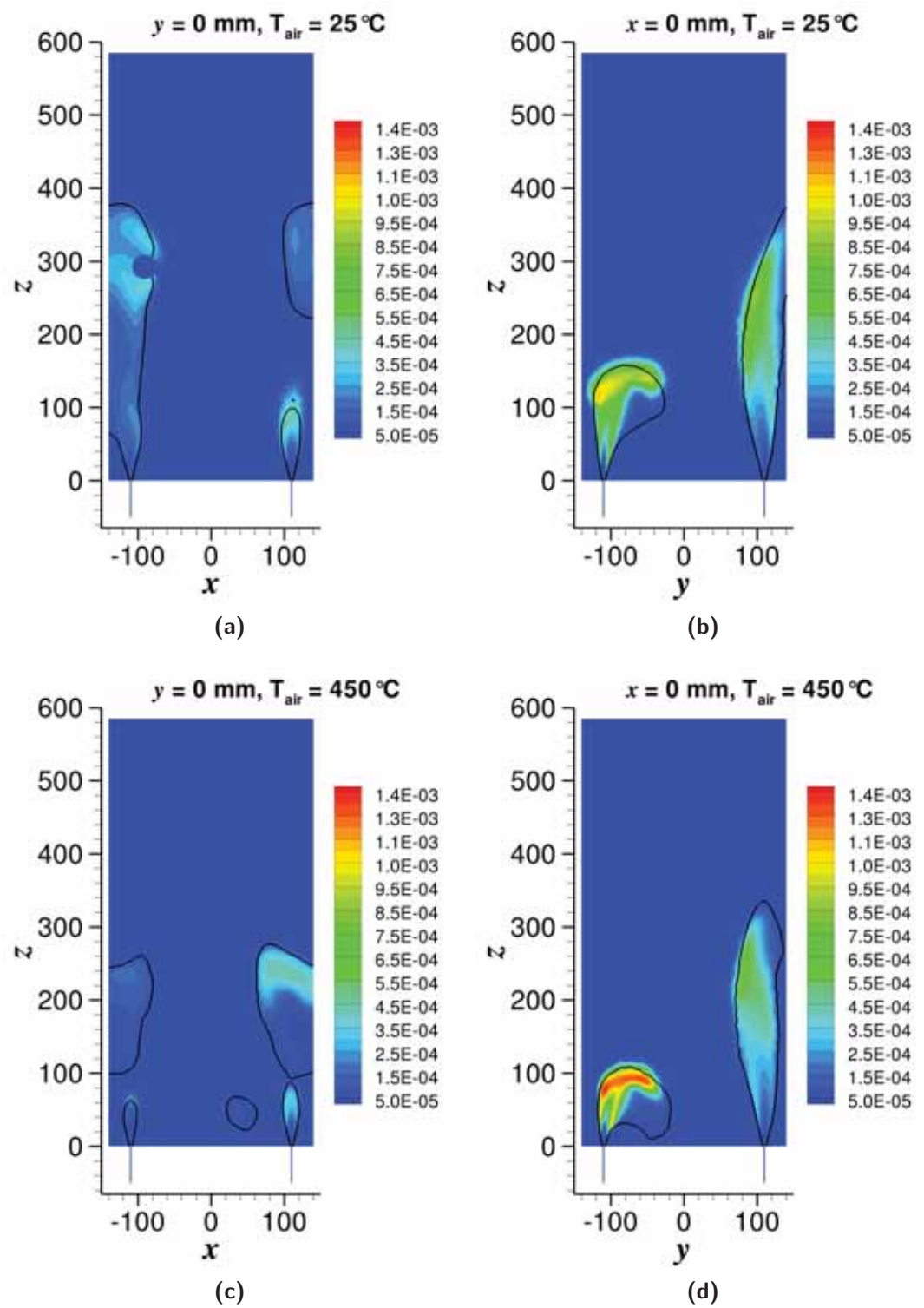

Figure F.9: Predicted CH_2O mole fraction contours with stoichiometric surface ($\xi_{st} = 0.0552$) overlaid for the baseline case, (a) and (b) without air preheat, $T_{air} = 25°C$, and (c) and (d) with air preheat, $T_{air} = 450°C$, for the EDC model with the Smooke mechanism at the $x - z$ and $y - z$ centreline planes.

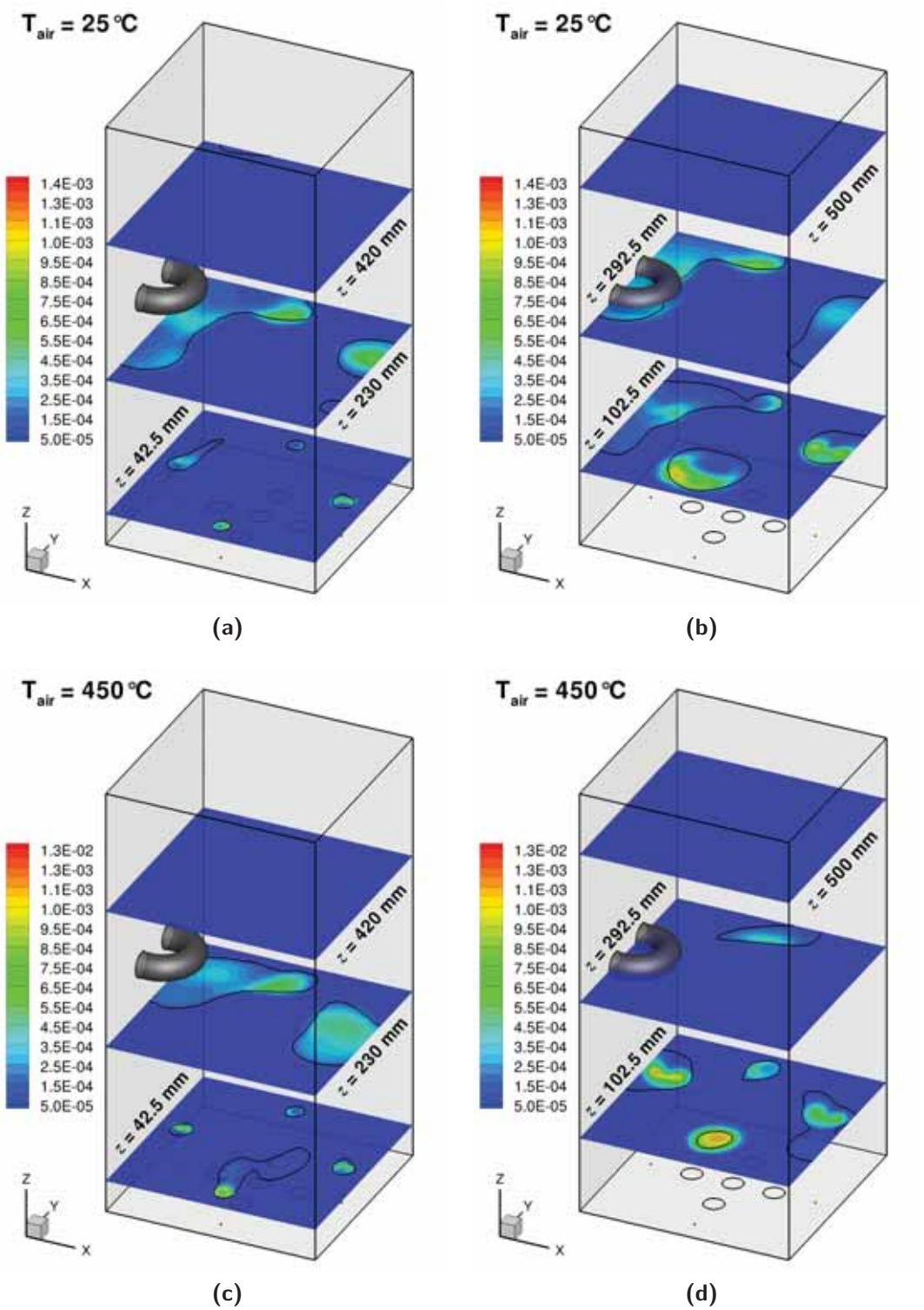

Figure F.10: Predicted CH_2O mole fraction contours with stoichiometric surface ($\xi_{st} = 0.0552$) overlaid for the baseline case, (a) and (b) without air preheat, $T_{air} = 25°C$, and (c) and (d) with air preheat, $T_{air} = 450°C$, for the EDC model with the Smooke mechanism at different $x - y$ planes.

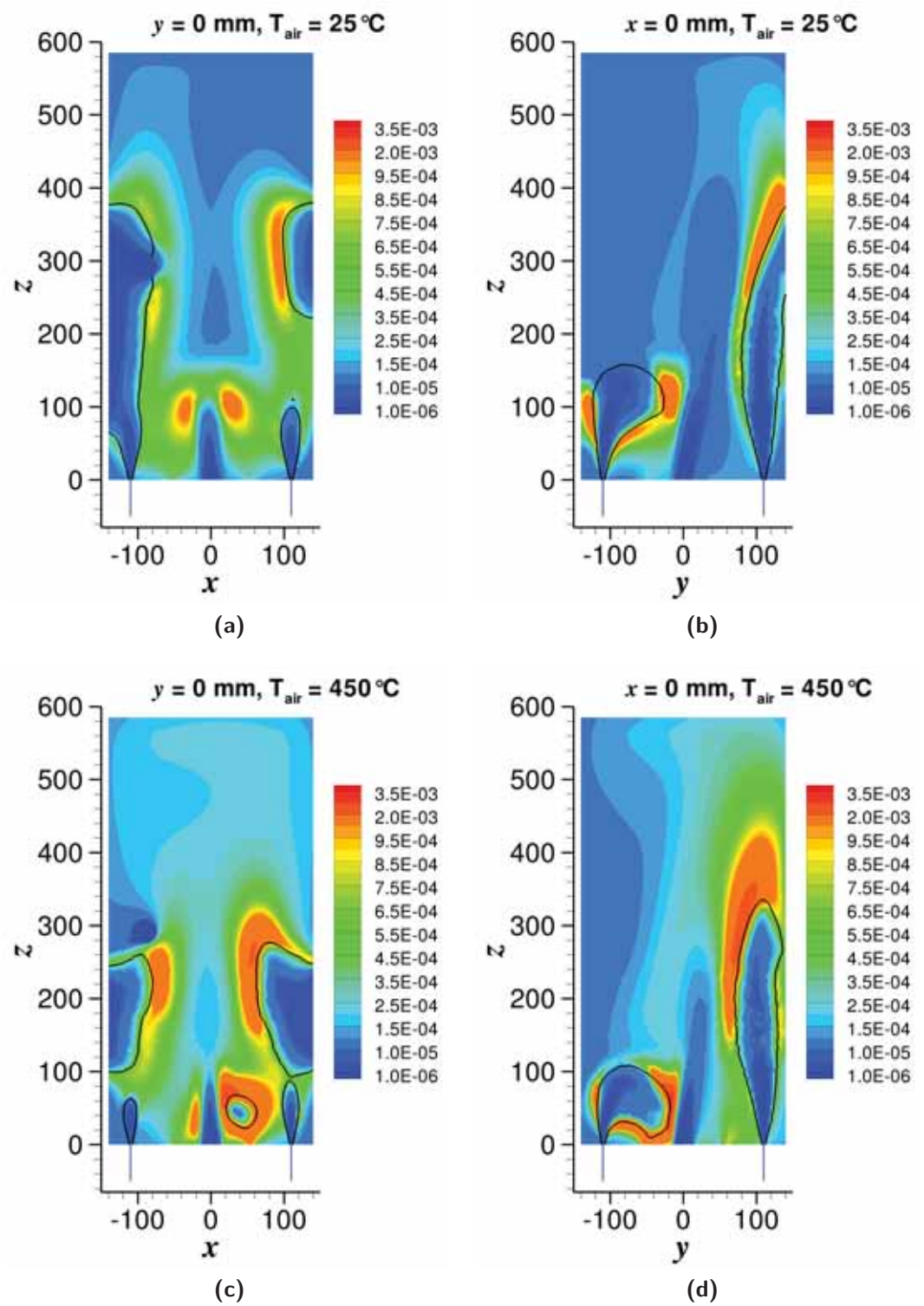

Figure F.11: Predicted OH mole fraction contours with stoichiometric surface ($\xi_{st} = 0.0552$) overlaid for the baseline case, (a) and (b) without air preheat, $T_{air} = 25°C$, and (c) and (d) with air preheat, $T_{air} = 450°C$, for the EDC model with the Smooke mechanism at the $x - z$ and $y - z$ centreline planes.

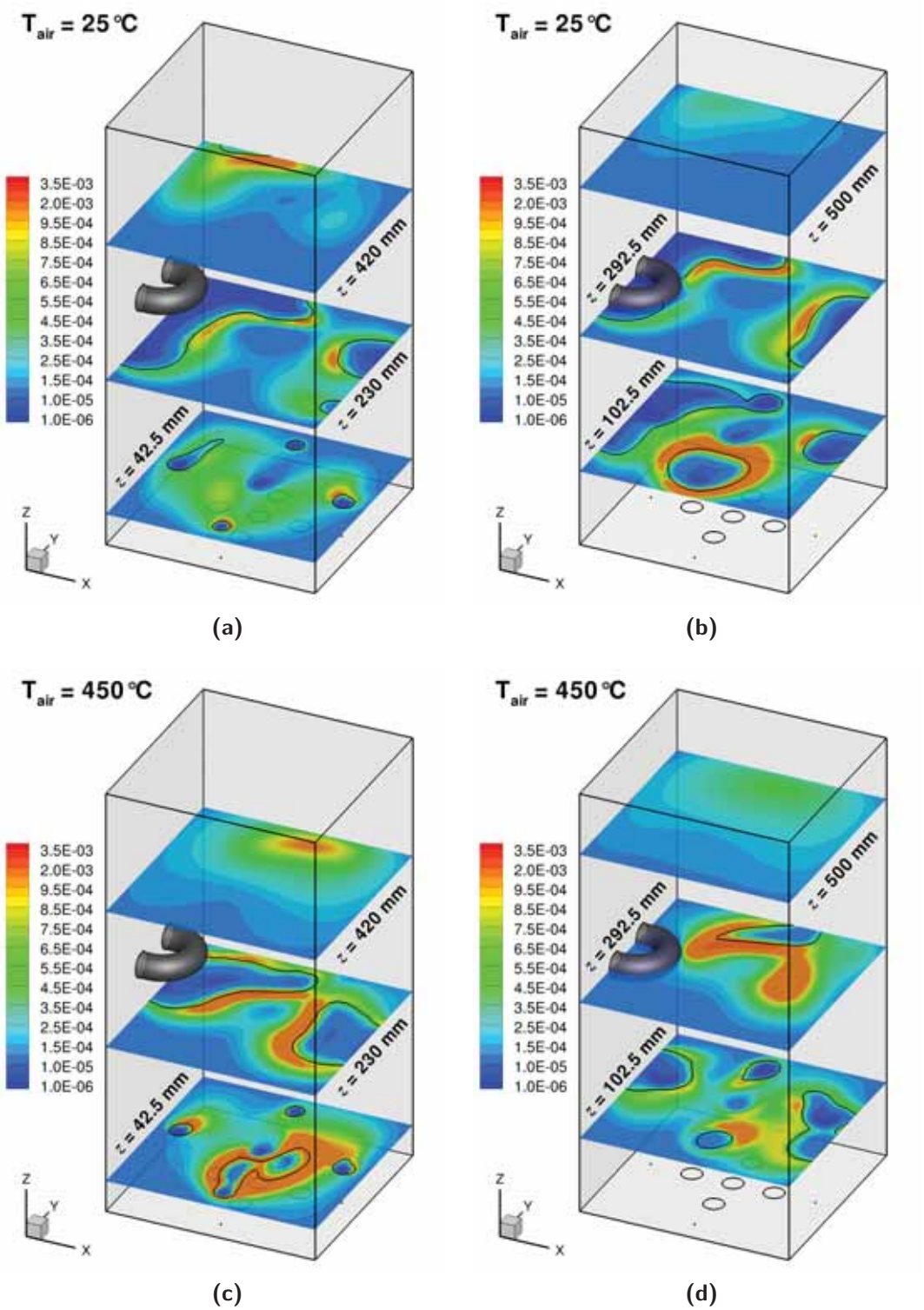

Figure F.12: Predicted OH mole fraction contours with stoichiometric surface ($\xi_{st} = 0.0552$) overlaid for the baseline case, (a) and (b) without air preheat, $T_{air} = 25°C$, and (c) and (d) with air preheat, $T_{air} = 450°C$, for the EDC model with the Smooke mechanism at different $x - y$ planes.

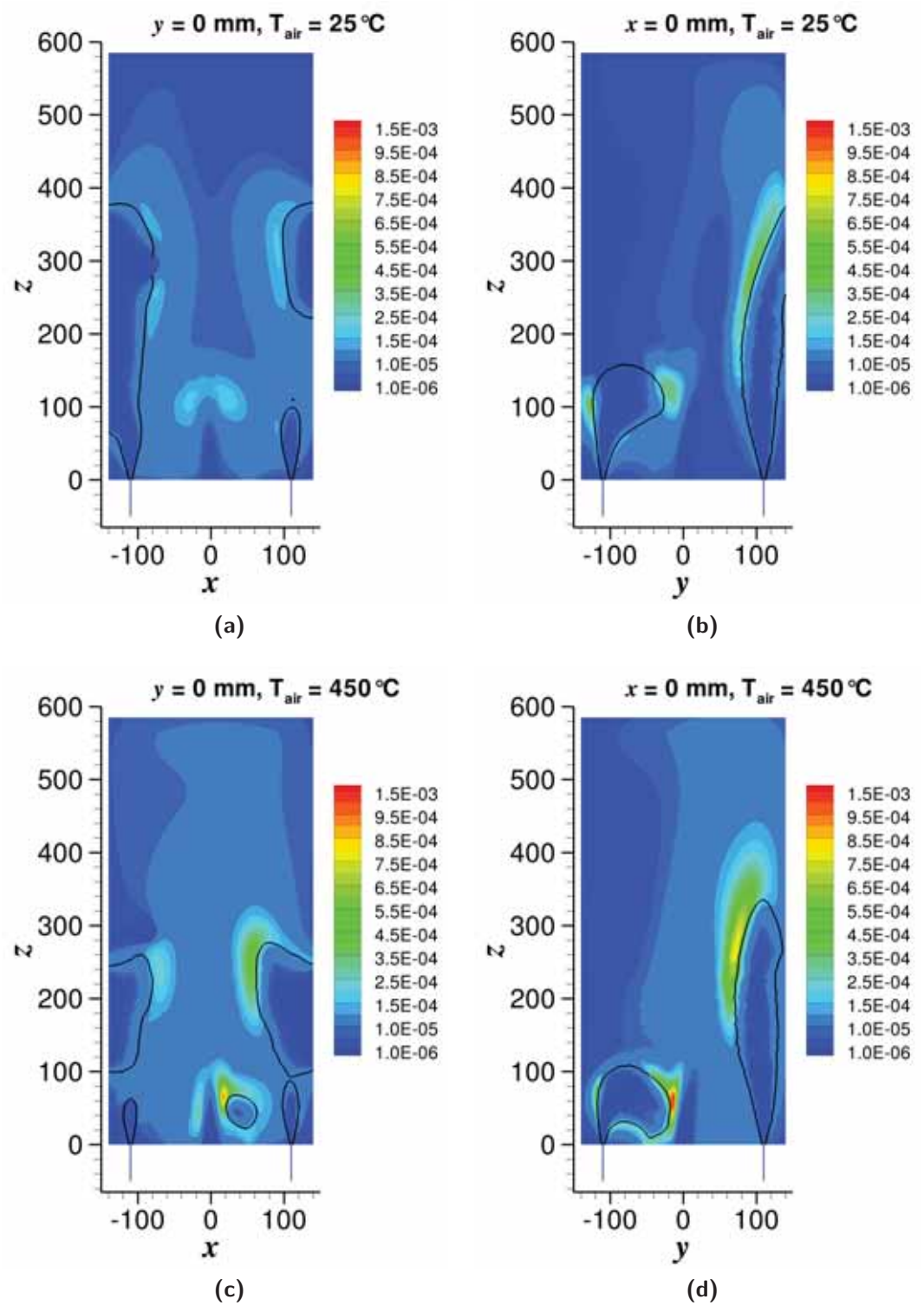

Figure F.13: Predicted O mole fraction contours with stoichiometric surface ($\xi_{st} = 0.0552$) overlaid for the baseline case, (a) and (b) without air preheat, $T_{air} = 25°C$, and (c) and (d) with air preheat, $T_{air} = 450°C$, for the EDC model with the Smooke mechanism at the $x - z$ and $y - z$ centreline planes.

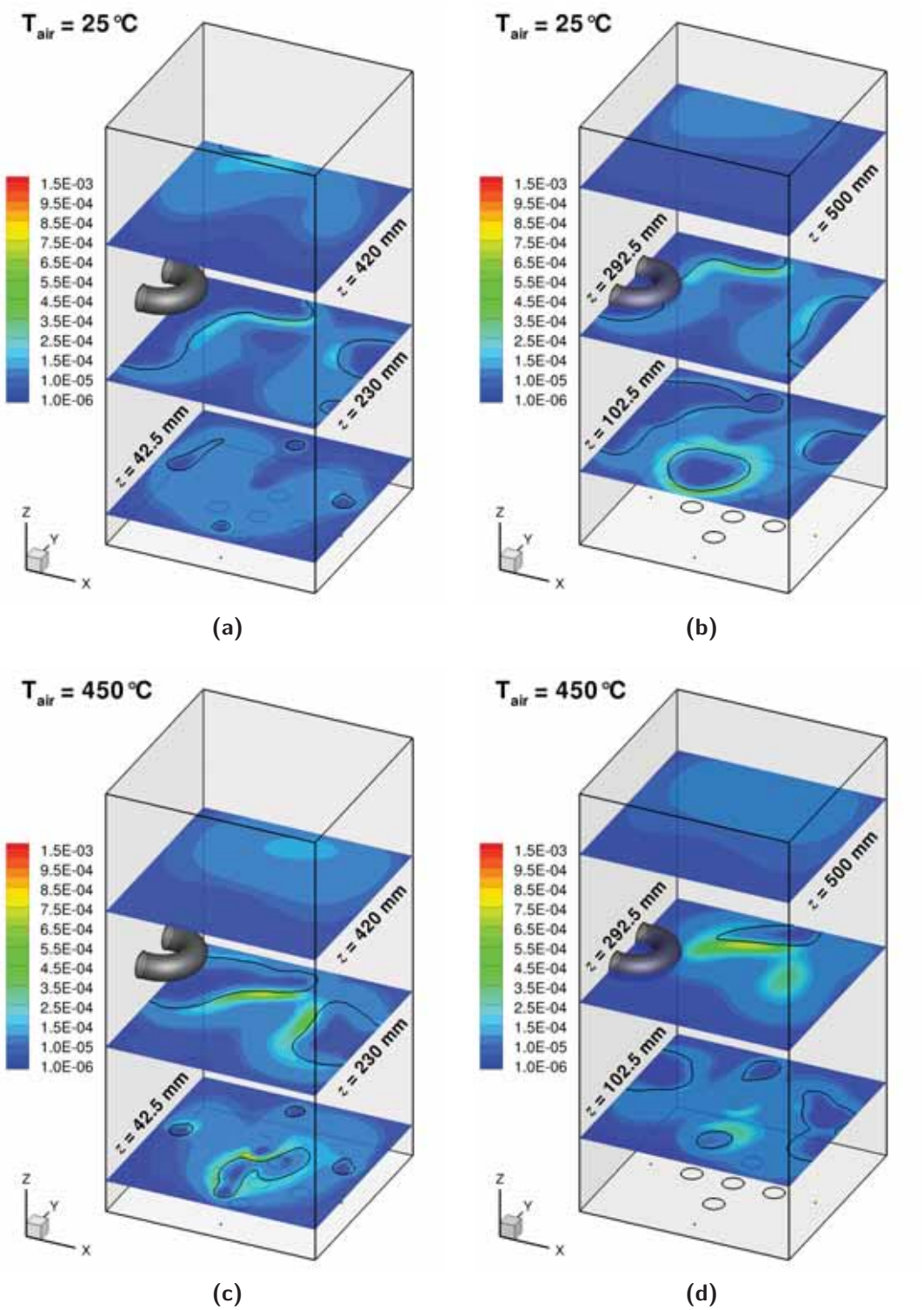

Figure F.14: Predicted O mole fraction contours with stoichiometric surface ($\xi_{st} = 0.0552$) overlaid for the baseline case, (a) and (b) without air preheat, $T_{air} = 25°C$, and (c) and (d) with air preheat, $T_{air} = 450°C$, for the EDC model with the Smooke mechanism at different $x - y$ planes.

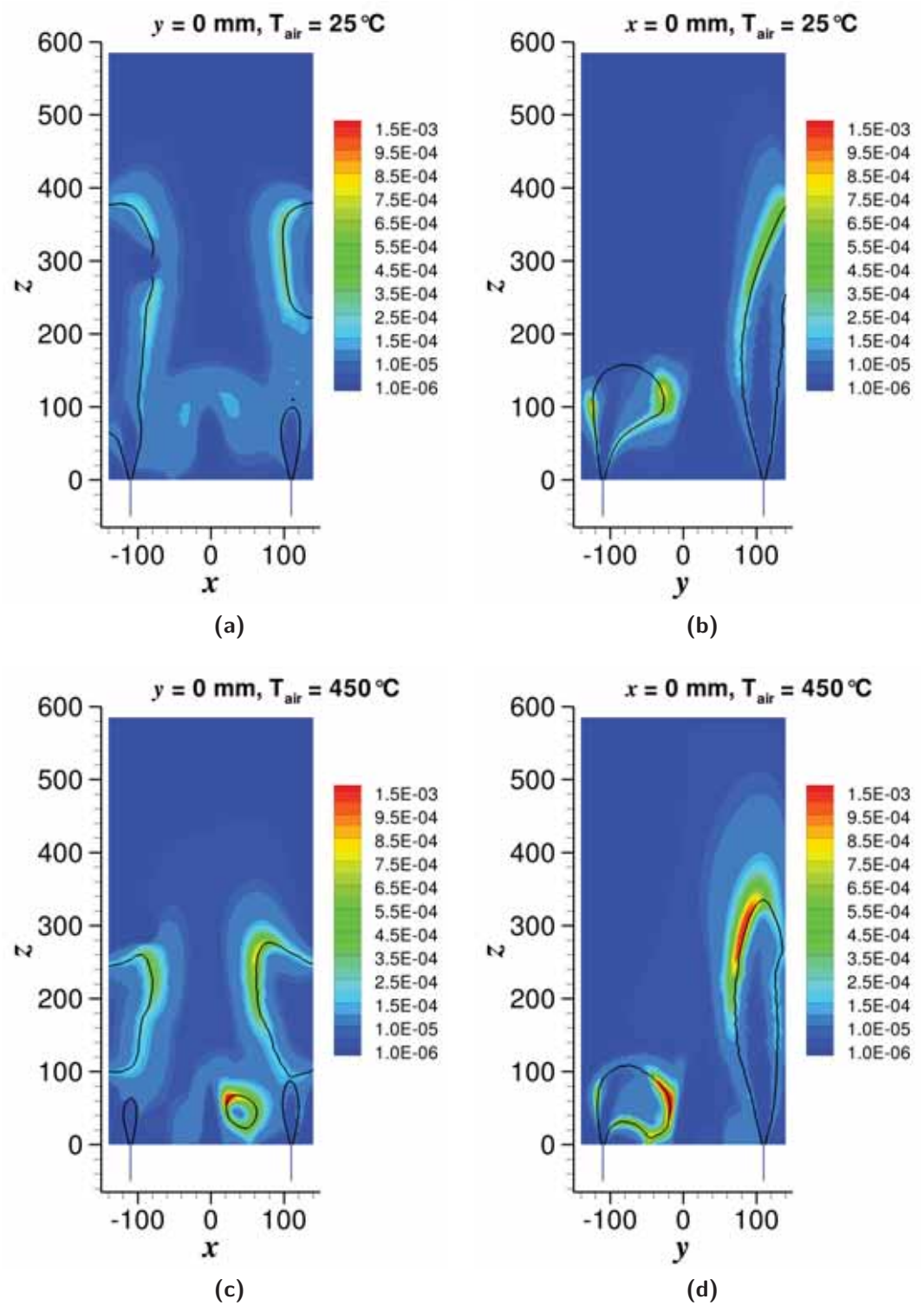

Figure F.15: Predicted H mole fraction contours with stoichiometric surface ($\xi_{st} = 0.0552$) overlaid for the baseline case, (a) and (b) without air preheat, $T_{air} = 25°C$, and (c) and (d) with air preheat, $T_{air} = 450°C$, for the EDC model with the Smooke mechanism at the $x - z$ and $y - z$ centreline planes.

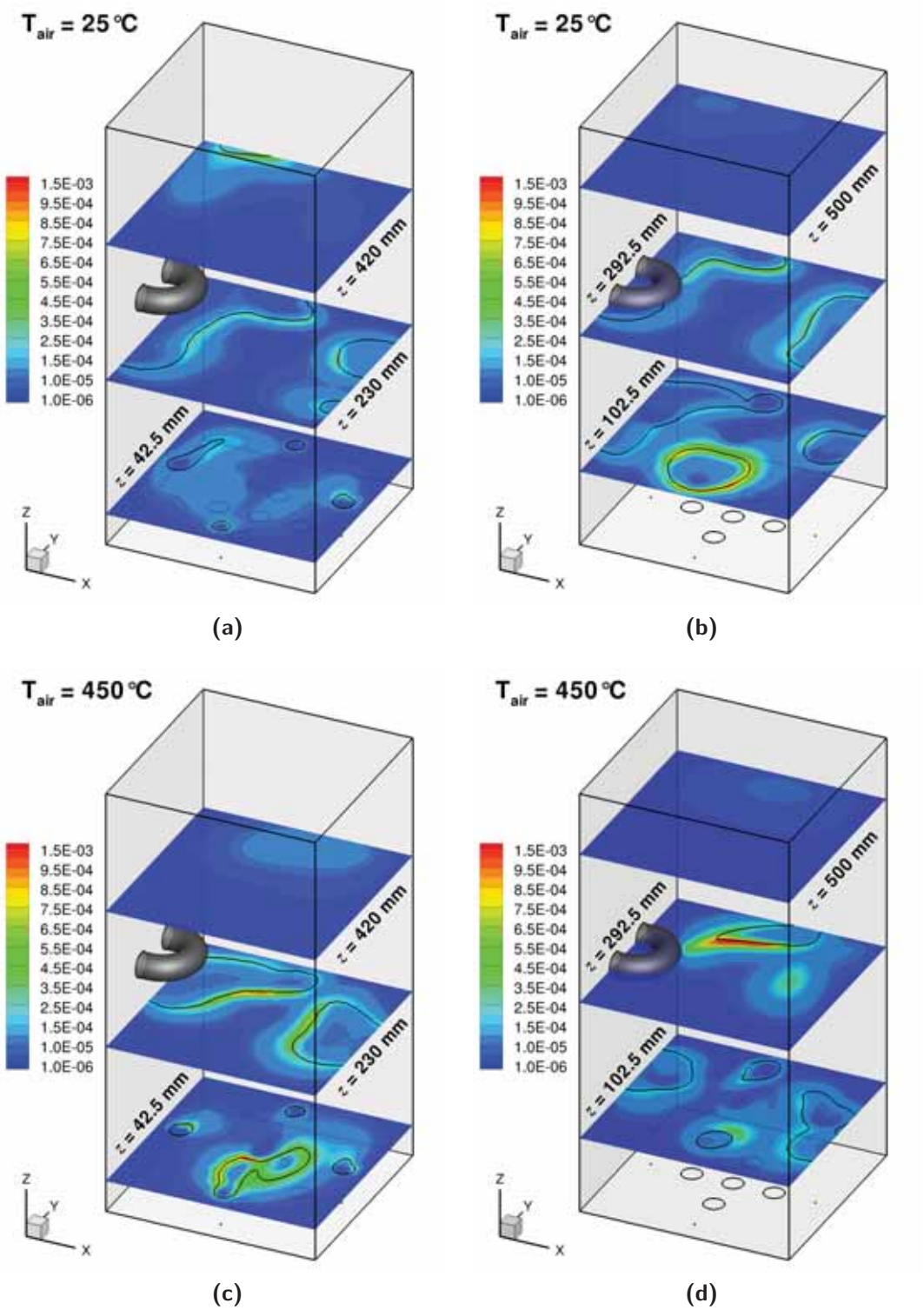

Figure F.16: Predicted H mole fraction contours with stoichiometric surface ($\xi_{st} = 0.0552$) overlaid for the baseline case, (a) and (b) without air preheat, $T_{air} = 25°C$, and (c) and (d) with air preheat, $T_{air} = 450°C$, for the EDC model with the Smooke mechanism at different $x - y$ planes.

Appendix G NO_x Contours

It must be noted that the mole fraction contours of all species presented in this Appendix are displayed on a wet basis.

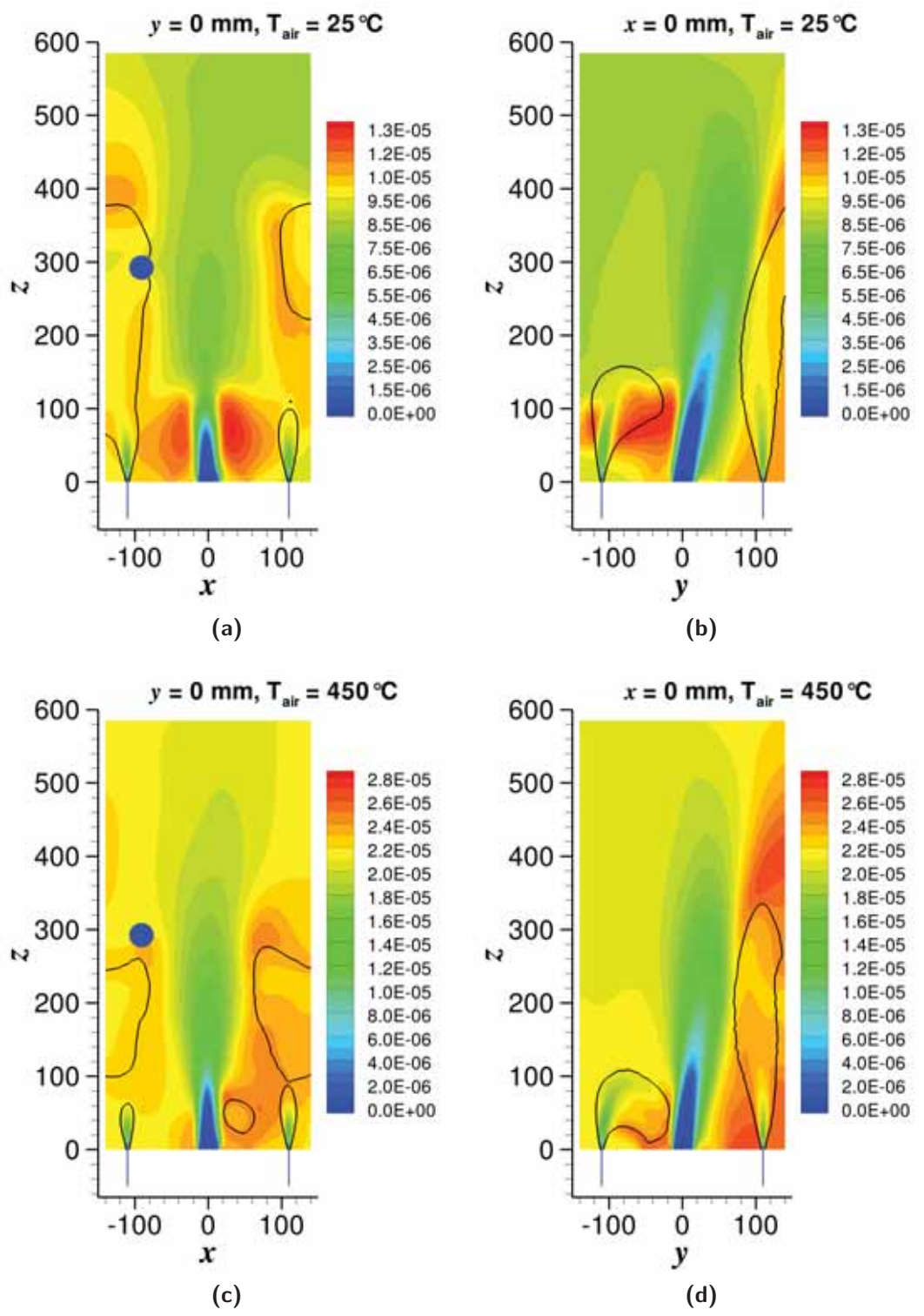

Figure G.1: Predicted NO mole fraction contours on a wet basis with stoichiometric surface ($\xi_{st} = 0.0552$) overlaid for the baseline case, (a) and (b) without air preheat, $T_{air} = 25°C$, and (c) and (d) with air preheat, $T_{air} = 450°C$, for the EDC model with the Smooke mechanism at the $x-z$ and $y-z$ centreline planes.

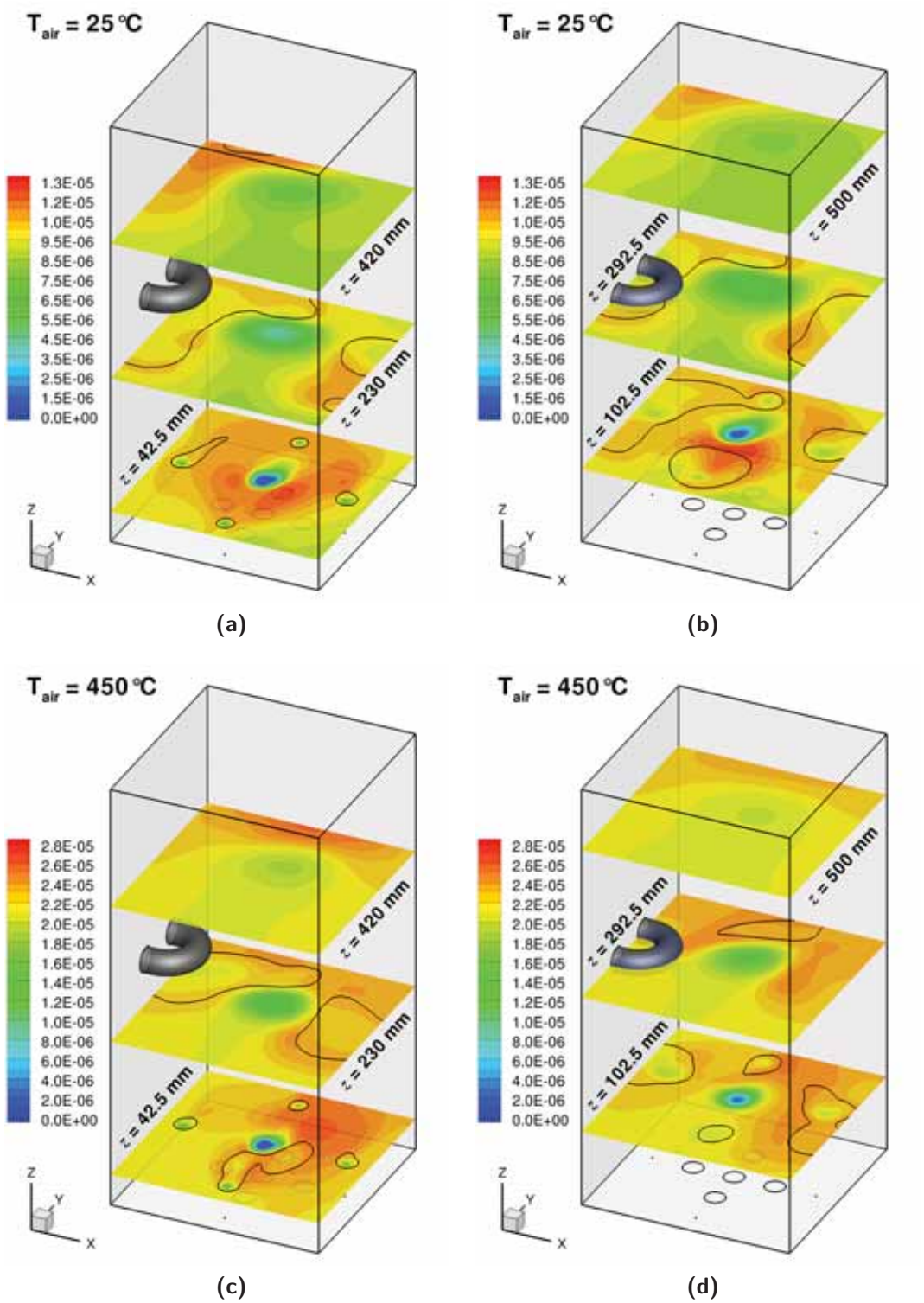

Figure G.2: Predicted NO mole fraction contours on a wet basis with stoichiometric surface ($\xi_{st} = 0.0552$) overlaid for the baseline case, (a) and (b) without air preheat, $T_{air} = 25°C$, and (c) and (d) with air preheat, $T_{air} = 450°C$, for the EDC model with the Smooke mechanism at different $x - y$ planes.

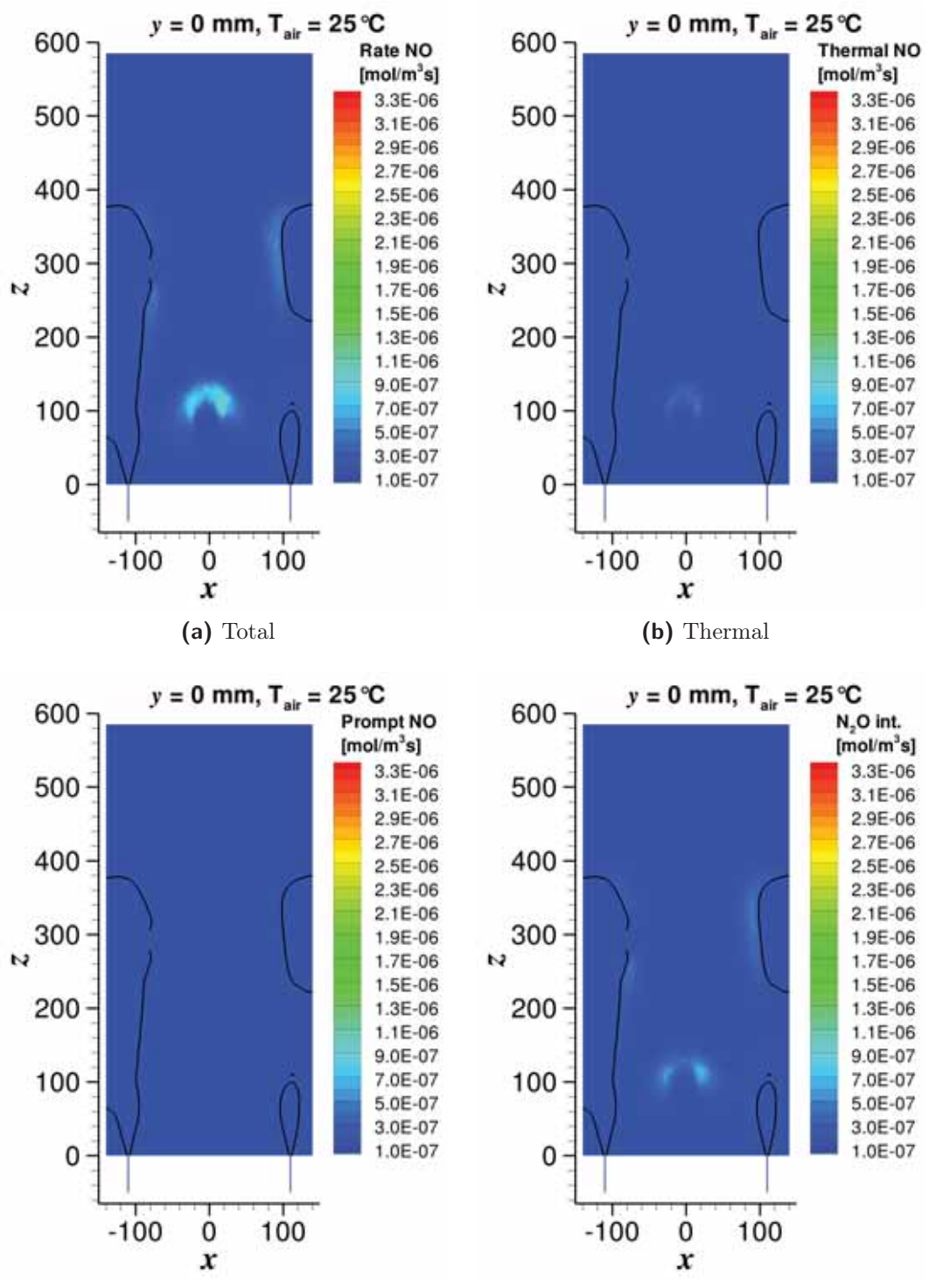

(a) Total

(b) Thermal

(c) Prompt

(d) N_2O-intermediate

Figure G.3: Predicted NO reaction rate contours with stoichiometric surface ($\xi_{st} = 0.0552$) overlaid for the baseline case without air preheat, $T_{air} = 25°C$, for the EDC model with the Smooke mechanism at the $x - z$ centreline plane. The thermal, prompt and N_2O-intermediate NO_x models were considered (Full NO case shown in Table 7.2).

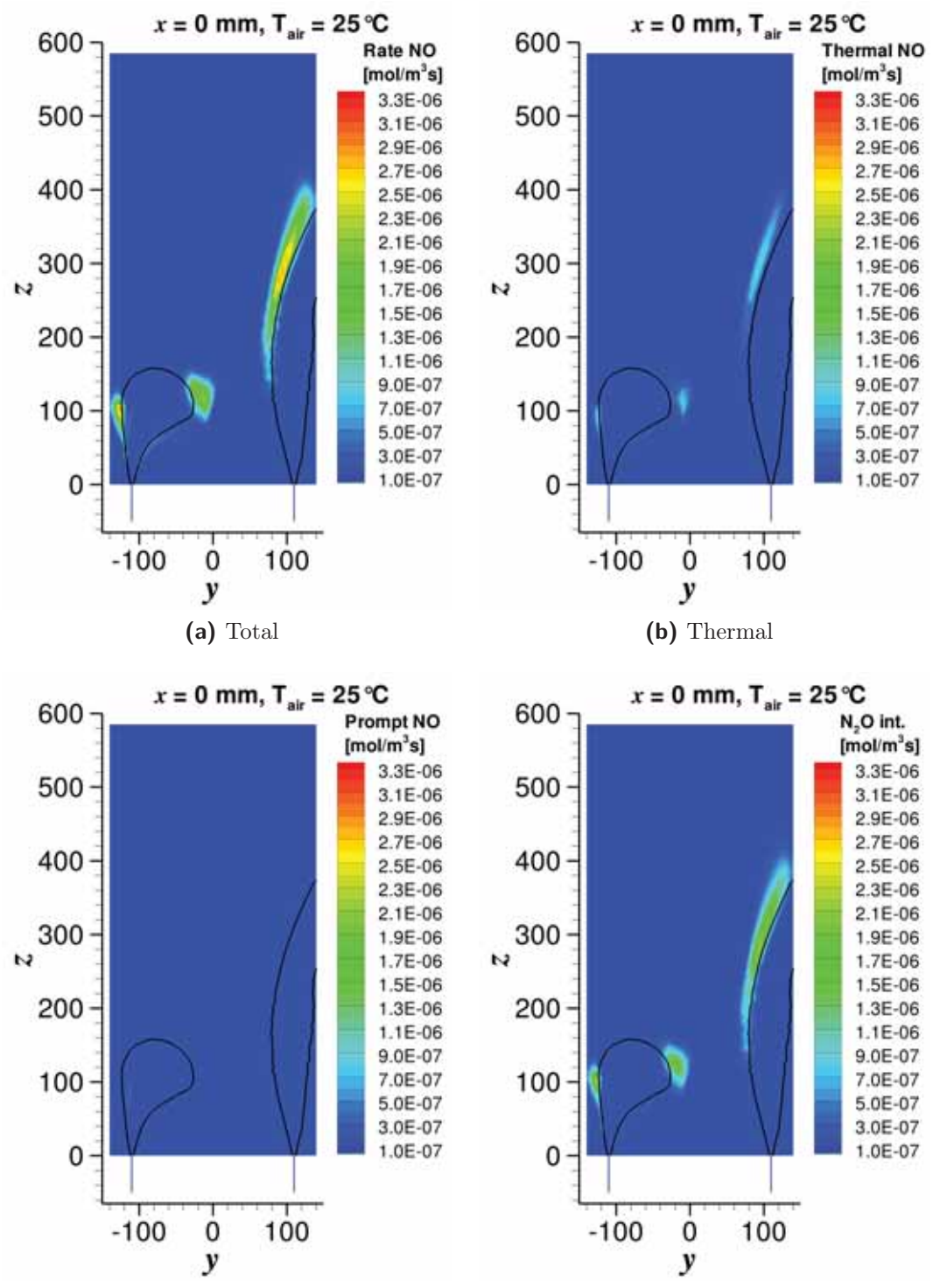

(a) Total **(b)** Thermal

(c) Prompt **(d)** N_2O-intermediate

Figure G.4: Predicted NO reaction rate contours with stoichiometric surface ($\xi_{st} = 0.0552$) overlaid for the baseline case without air preheat, $T_{air} = 25°C$, for the EDC model with the Smooke mechanism at the $y - z$ centreline plane. The thermal, prompt and N_2O-intermediate NO_x models were considered (Full NO case shown in Table 7.2).

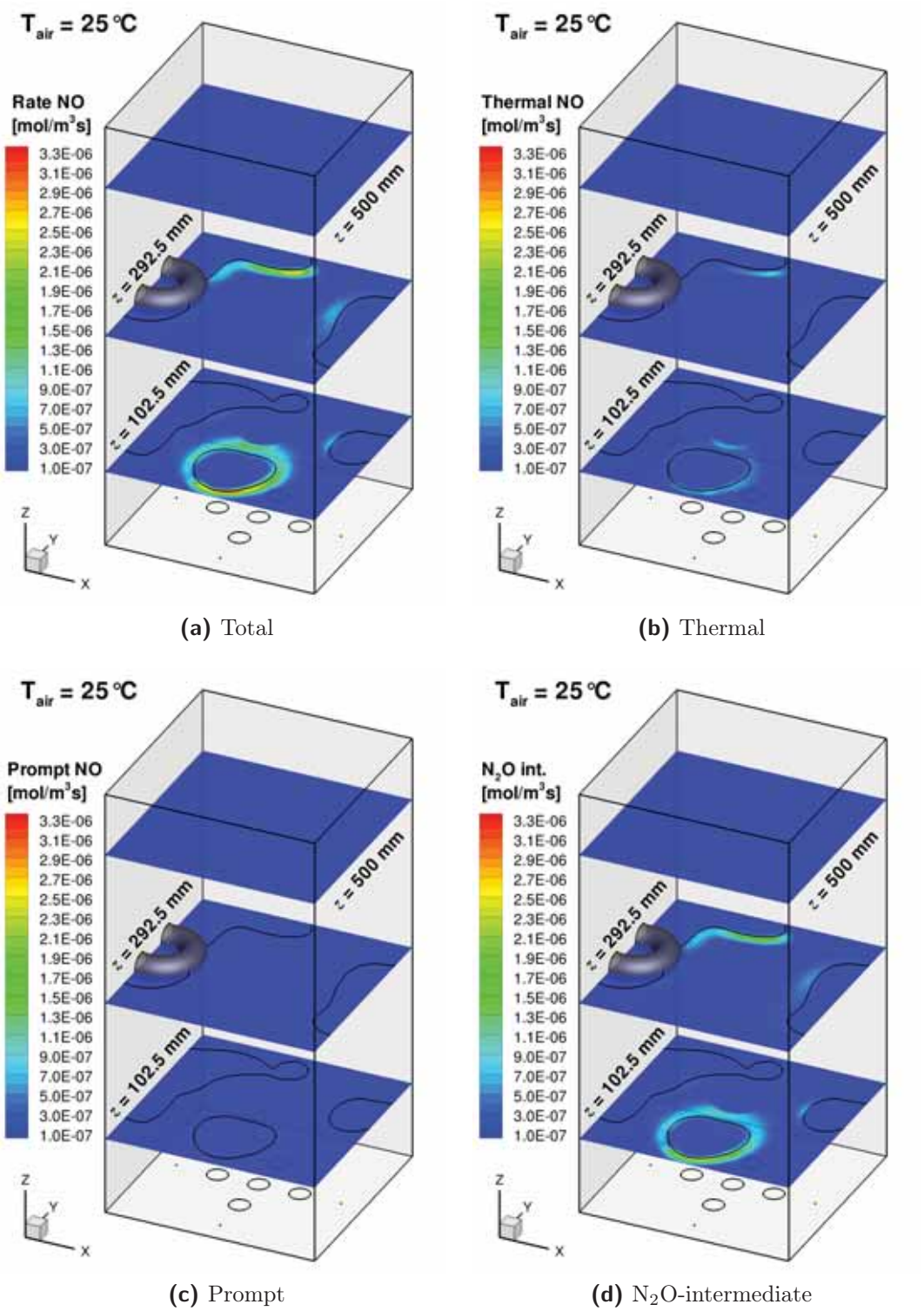

(a) Total **(b)** Thermal

(c) Prompt **(d)** N_2O-intermediate

Figure G.5: Predicted NO reaction rate contours with stoichiometric surface ($\xi_{st} = 0.0552$) overlaid for the baseline case without air preheat, $T_{air} = 25°C$, for the EDC model with the Smooke mechanism at different $x - y$ planes. The thermal, prompt and N_2O-intermediate NO_x models were considered (Full NO case shown in Table 7.2).

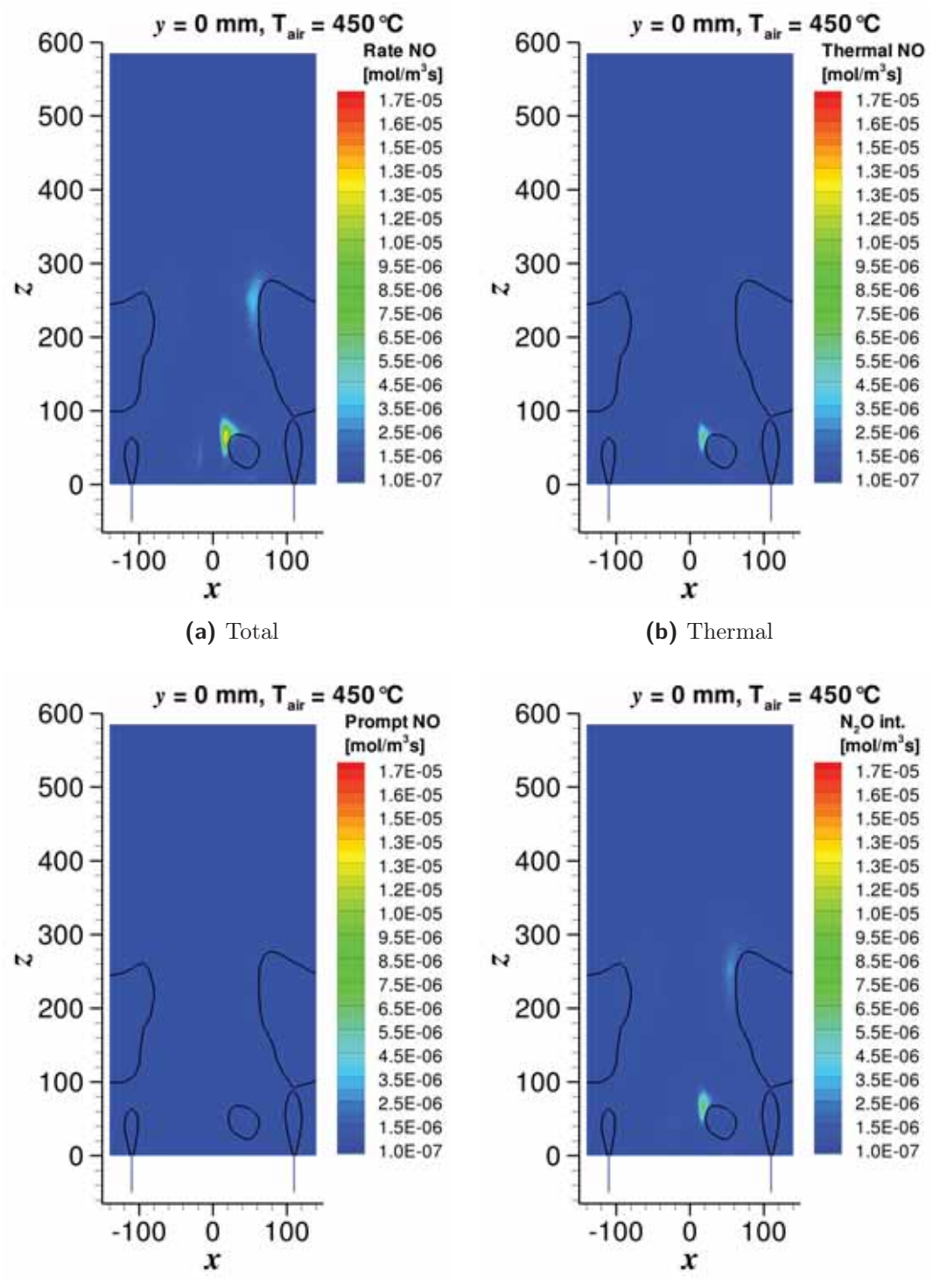

(a) Total **(b)** Thermal

(c) Prompt **(d)** N_2O-intermediate

Figure G.6: Predicted NO reaction rate contours with stoichiometric surface ($\xi_{st} = 0.0552$) overlaid for the baseline case with air preheat, $T_{air} = 450°C$, for the EDC model with the Smooke mechanism at the $x - z$ centreline plane. The thermal, prompt and N_2O-intermediate NO_x models were considered (Full NO case shown in Table 7.2).

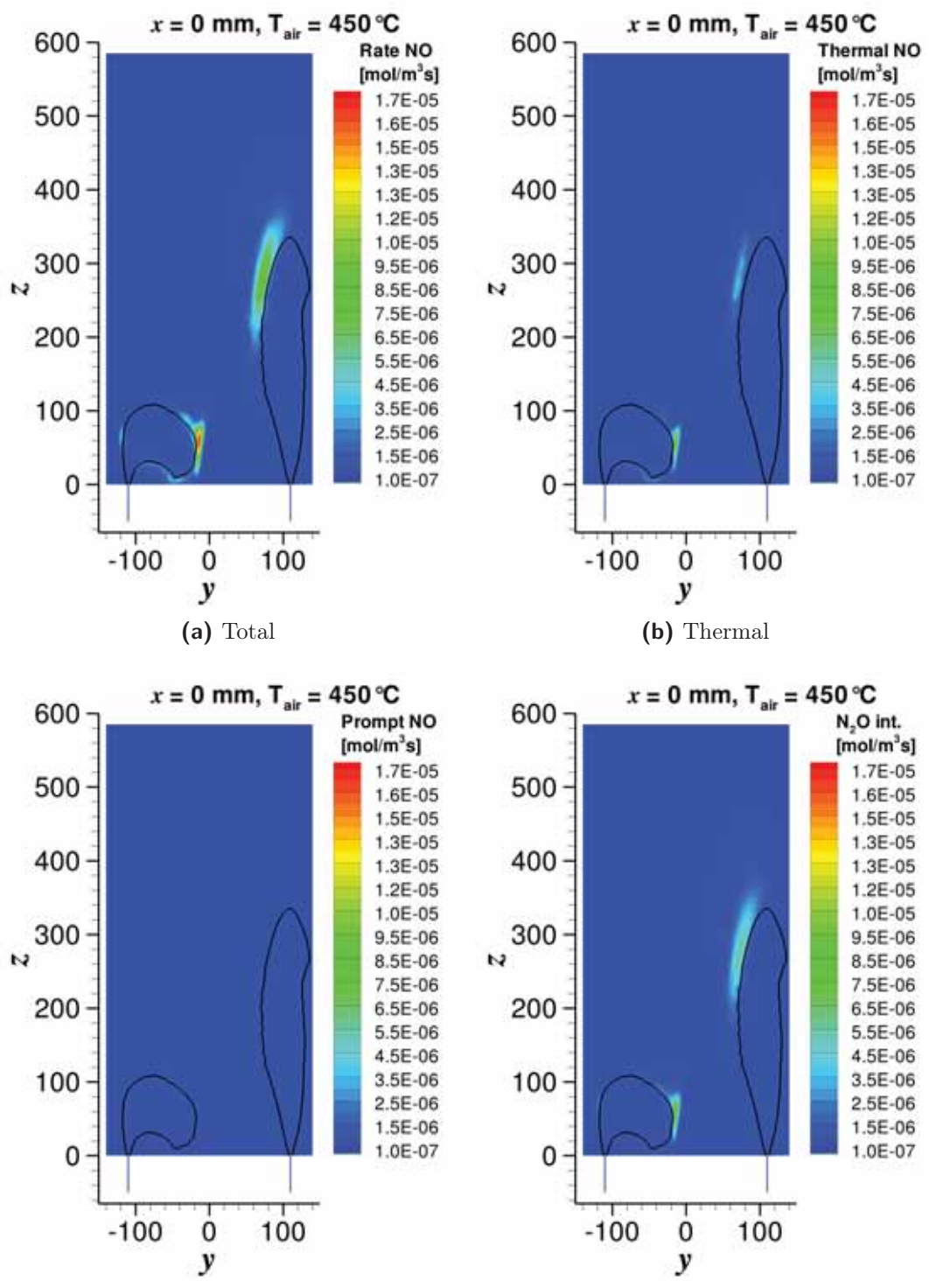

(a) Total

(b) Thermal

(c) Prompt

(d) N_2O-intermediate

Figure G.7: Predicted NO reaction rate contours with stoichiometric surface ($\xi_{st} = 0.0552$) overlaid for the baseline case with air preheat, $T_{air} = 450°C$, for the EDC model with the Smooke mechanism at the $y - z$ centreline plane. The thermal, prompt and N_2O-intermediate NO_x models were considered (Full NO case shown in Table 7.2).

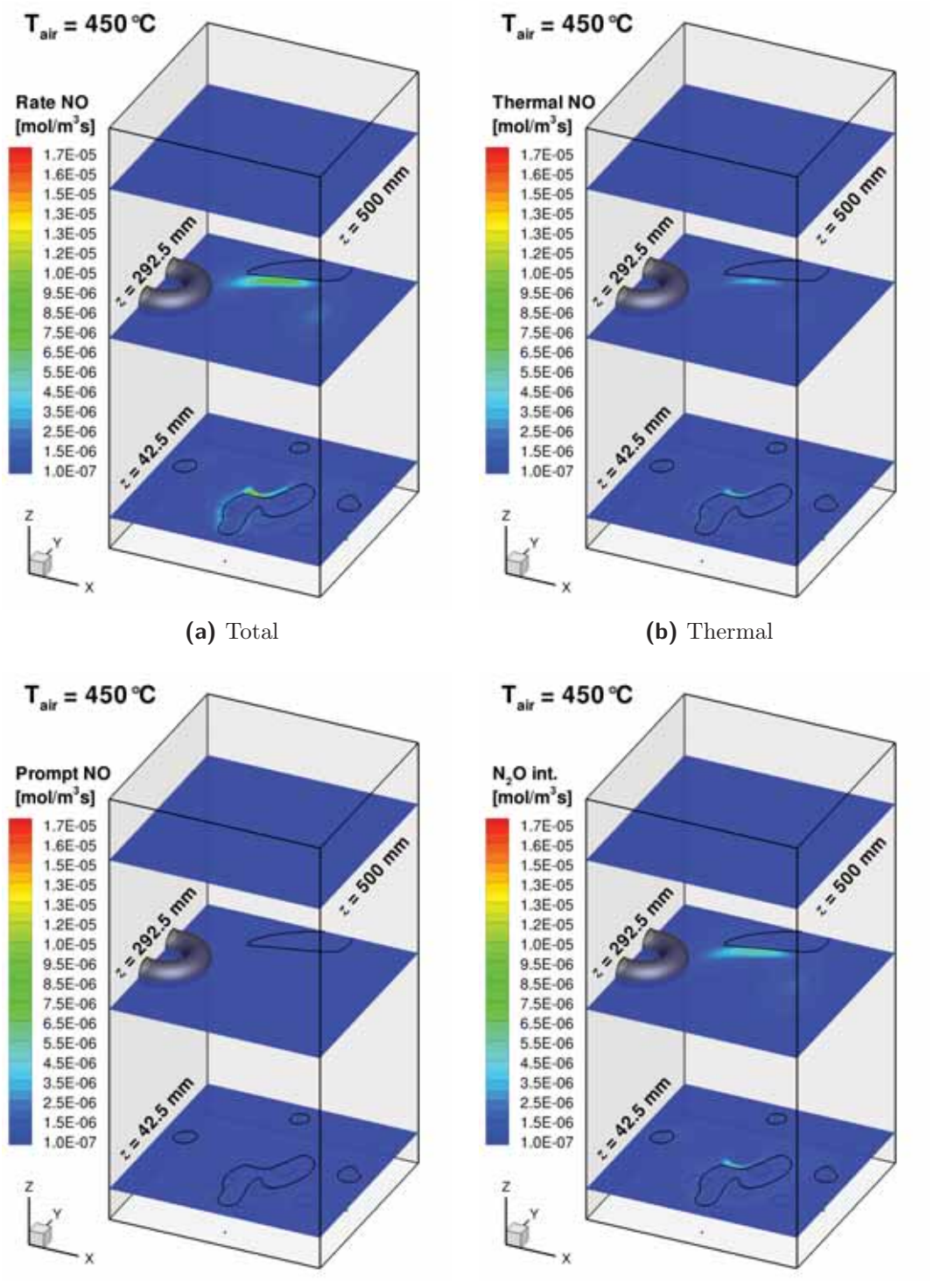

(a) Total **(b)** Thermal

(c) Prompt **(d)** N_2O-intermediate

Figure G.8: Predicted NO reaction rate contours with stoichiometric surface ($\xi_{st} = 0.0552$) overlaid for the baseline case with air preheat, $T_{air} = 450°C$, for the EDC model with the Smooke mechanism at different $x - y$ planes. The thermal, prompt and N_2O-intermediate NO_x models were considered (Full NO case shown in Table 7.2).

Appendix H Publications

Publications arising from this thesis

G. G. Szegö, B. B. Dally, G. J. Nathan, F. C. Christo, Design optimisation of a MILD combustion furnace based on CFD modelling, in: Proceedings of the Australian Symposium on Combustion and the Eighth Australian Flame Days, No. P047, Monash University, Melbourne, 2003.

G. G. Szegö, B. B. Dally, G. J. Nathan, F. C. Christo, Performance characteristics of a 20kW MILD combustion furnace, in: The Sixth Asia-Pacific Conference on Combustion, The Combustion Institute, Nagoya, Japan, 2007, pp. 231−234.

G. G. Szegö, B. B. Dally, G. J. Nathan, Stability limits of a parallel jet MILD combustion burner system, in: Proceedings of the Australian Combustion Symposium, University of Sydney, 2007, pp. 62−65.

G. G. Szegö, B. B. Dally, G. J. Nathan, Experimental investigation of a parallel jet MILD combustion burner system, in: The Seventh High Temperature Air Combustion and Gasification International Symposium, Phuket, Thailand, 2008.

G. G. Szegö, B. B. Dally, G. J. Nathan, Scaling of NO_x emissions from a laboratory-scale MILD combustion furnace, Combustion and Flame 154 (1−2) (2008) 281−295.

G. G. Szegö, B. B. Dally, G. J. Nathan, Operational characteristics of a parallel jet MILD combustion burner system, Combustion and Flame 156 (2) (2009) 429−438.

G. G. Szegö, B. B. Dally, F. Christo, Investigation of the mixing patterns inside a MILD combustion furnace based on CFD modelling, in: Proceedings of the Australian Combustion Symposium, University of Queensland, 2009.